Tool Stickout Optimization

Table of contents

This project is made in collaboration with:

Funding:

Industry partners:

V. BECH TOOLS

1 Executive Summary

Chatter vibration is one of the most difficult and unpredictable challenges the mechanical industry faces. Since the birth and apogee of high-speed milling, several approaches have been developed to mitigate this complex phenomenon.

This report provides a comprehensive study of how stability and self-exited vibration areas shift when a change in the tool stickout is introduced. Several tests were conducted and the inverse relationship between stickout and system´s natural frequencies was observed. Setting a number of conditions, it was possible to predict the frequency shifting. This opens an improvement window that potentially allows companies to tune their machines set up to achieve greater exploitation of their capacities.

A systematic method to collect tap test data was established giving a work frame for future research. Equations describing tool configurations were modelled and a method to get new algorithms can be extracted to progress even further.

During this study, we clearly saw another improvement field opening. To be able to shift lobes on the SLD gives a different approach to optimization processes, where the industry has the possibility of choosing between spindle speed or stickout variation to enhance productivity.

2 Introduction

Machining stands out as the most widely utilized metal-cutting process in the manufacturing sector, making it a captivating subject for research. This technique involves altering a raw material or workpiece into a desired shape and size through a pre-planned sequence of operations. Although metals currently dominate the realm of machined materials, this preference can differ by industry.

This manufacturing approach finds utility across diverse industries such as aerospace, construction, power, and numerous other sectors, each imposing unique requirements on the final product. Notably, machining can induce undesired vibrations during the process, thereby reducing production efficiency and the surface finish of the machined component. Both aspects hold significance for manufacturers, but achieving superior surface quality becomes imperative in industries where meeting stringent tolerances is obligatory, as seen in the defence and aerospace sectors. In reality, understanding these vibrations, known as chatter, has posed a significant challenge to the machining industry over the years.

2.1 Understanding vibrations

It is especially important to describe and understand the vibration phenomena before developing concepts any further. To start we must notice that vibrations are produced due to the interaction of the tool with the workpiece. Both elements are made of elastic bodies that deform when subjected to external forces. To simplify the study, in certain cases, we can consider the workpiece as a completely rigid element to focus our efforts on the cutting tool (the most flexible element). Thus, mechanical vibrations will be defined as the oscillating response of the tool's elastic body to disturbances. Depending on the characteristics of the excitation, the vibrations can be grouped into free, forced, and self-excited vibrations.

Free vibrations occur when the excitation acts on the elastic system for a discreet period and disappears. This type of vibration can be described with a basic SDOF (single-degree-of-freedom) model of mass,

spring, and damper. In this case, the system described by the parameters m (mass), k (rigidity), and c (damping); can be disturbed by moving the starting point a certain distance x (Figure 1).

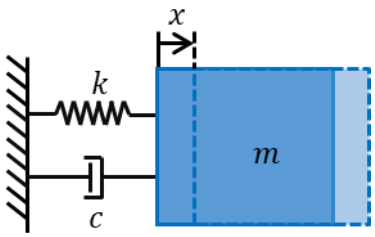

Figure 1 – Free vibration of a mass-spring-damper SDOF system.

After removing the disturbance, the following movement equation applies,

$$\sum F_X = m\ddot{x} + c\dot{x} + kx = 0$$

Immediately after the disturbance disappears the system will start oscillating. In terms of energy, the damper will start consuming all kinetic energy until the movement amplitude decreases to equilibrium (steady state). The movement amplitude described by the equation can be plotted over time (Figure 2).

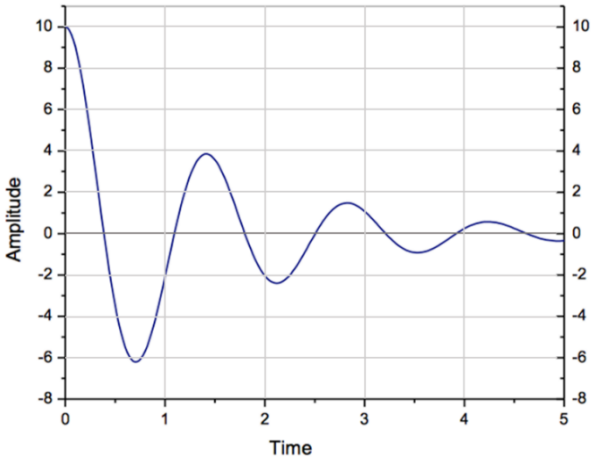

Figure 2 – Time response on free vibrations.

Alternatively, forced vibrations are found when the system is constantly exited by a periodic external force. These models can be represented by the same equation of motion, the only difference will be the sum of forces will not be equal to zero (see Figure 3).

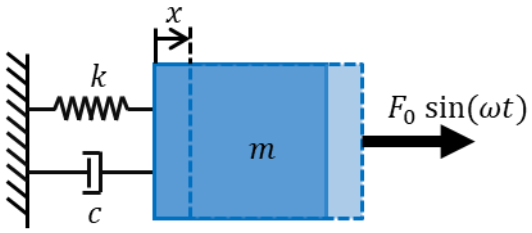

Figure 3 - Forced vibration of a mass-spring-damper SDOF system.

$$\sum F_X = m\ddot{x} + c\dot{x} + kx = F_0 \, cos \, cos \, (\omega t)$$

The typical solution or response from these systems can be divided into two segments: the transient and the permanent response. As we can see in Figure 4, after some time, the transient part decreases and the response converges to a steady state, matching the forcing frequency.

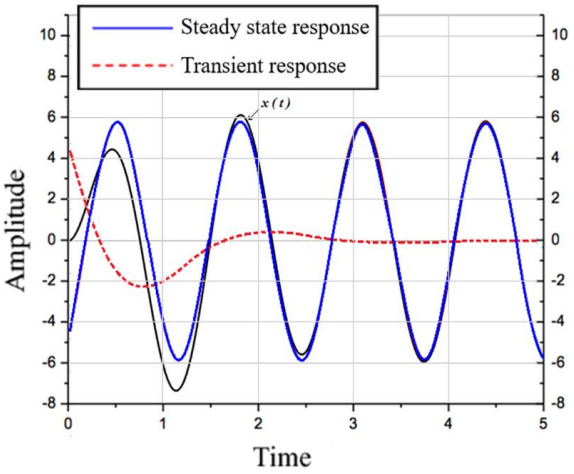

Figure 4 – Time response on forced vibration.

For the analysis, and due to the constant nature of the steady-state response, we can characterize the first stage of the systems only by the transient response. As we can anticipate the transient part of the response can have different convergent shapes. We call this tendency to converge “damping coefficient”.

Lastly, it is crucial to mention self-exited vibrations. This vibration type is produced when the modal parameters produce a self-sustained oscillation response with a greater amplitude. To sum up, in self-excited vibrations, the system interacts with itself in a feedback loop, generating its own source of vibration without continuous external excitation. Chatter, that infamous and disruptive vibration in CNC milling, is a prime example of self-excited vibrations. It occurs when the machining process induces vibrations that feedback into the system, causing it to vibrate at its natural frequencies, often unpredictably and with detrimental consequences.

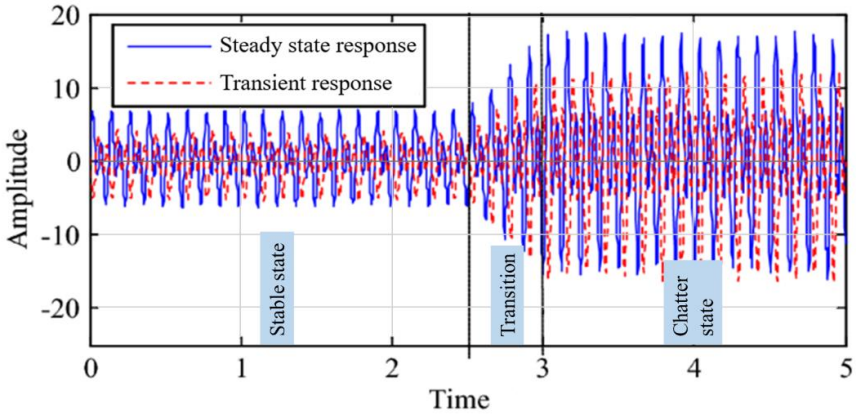

Figure 5 - Time response for self-exited vibrations.

2.2 A practical approach to chatter suppression

Effective chatter control strategies, such as tool selection, cutting parameter optimization, machine rigidity enhancement, and advanced machining techniques, all hinge on a deep understanding of these vibrations. It's this knowledge that allows us to push the boundaries of precision, productivity, and quality while navigating the complex world of vibrations in machining.

The first natural reaction to chatter occurrence is to reduce spindle speed and/or depth of cut. This solution has an obvious negative impact on production. DAMRC already has extensive knowledge about giving solutions to suppress these undesirable vibrations and, at the same time, delivering a superior cut.

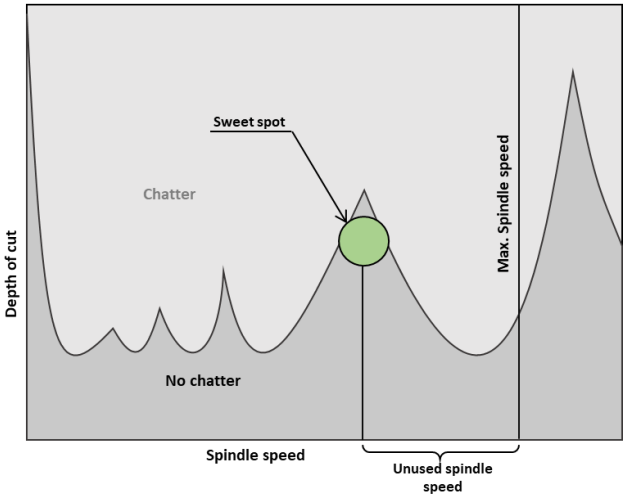

Figure 6 - Stability lobe diagram sweet spot optimization.

Another common response to avoid chatter is to switch to a tool with a smaller length-to-diameter ratio. In most cases, this is an effective response but, in some cases, doing the opposite will represent an advantage.

The tool stickout is defined as the length by which the tool extends from the tool holder. Many spindles allow the operator to change this value. Doing so can allow industries that are already performing stable high-speed milling to achieve even greater productivity.

The main limitation of machining at a stable speed is that the maximum speed is unused due to the low permitted depth of cut in this work area. Even after a tuning process, the most productive “sweet spot” is usually located way below the maximum machine speed limit.

Changing the tool stickout produces an effect on the stability diagram, a longer stickout will shift the lobe located outside of the machine spindle speed limits to lower speeds. Selecting the precise tool stickout may shift the lobe the necessary amount to locate it inside the machine's working area. This would represent a new sweet spot with much greater material removal properties.

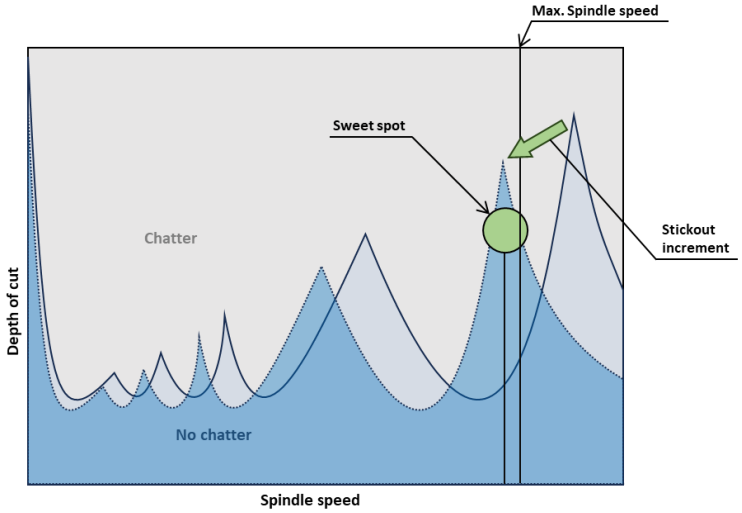

Figure 7 - Frequency shifting on a stability lobe diagram.

In some practical industry cases a long stickout is mandatory (e.g., deep pocket operations) in those cases the importance of selecting the correct stickout could represent a game-changing factor. The natural tendency is to select the necessary stickout to avoid collision with the workpiece. Several studies have confirmed the possibility of finding a more stable productivity area in those conditions.

3 Pre-analysis and Literature search

Every combination of machine, tool holder, collet, and milling tool represents a system with its natural frequencies, stiffness, damping, and mass values. The frequency response function (FRF) model is the foundation to get these values, this function can be obtained by introducing an input to a specific machine system configuration and processing the results.

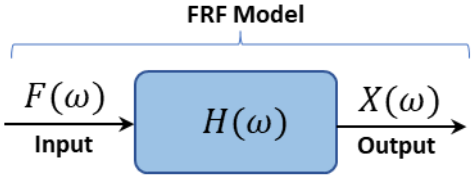

Figure 8 - Frequency response model block diagram.

The method used in this case is tap test, this test involves a sensor affixed to the combination of machine and tooling that makes up the machining system, along with a calibrated hammer for tapping this system and an analysis tool for measuring the frequency response.

An FRF measurement conducted on any structure will reveal a series of peaks in its response. These individual peaks are often distinct and possess identifiable centre frequencies, indicating that they correspond to resonances. Each resonance typically mirrors the response of a single-degree-of-freedom (SDOF) structure. When the broader peaks in the FRF are examined with higher frequency resolution, it's common to find two or more resonances closely grouped together. This suggests that the structure can be understood as a collection of SDOF substructures. This forms the foundation of modal analysis, a technique used to analyse a structure's behaviour by identifying and assessing all the resonances or modes present in its response.

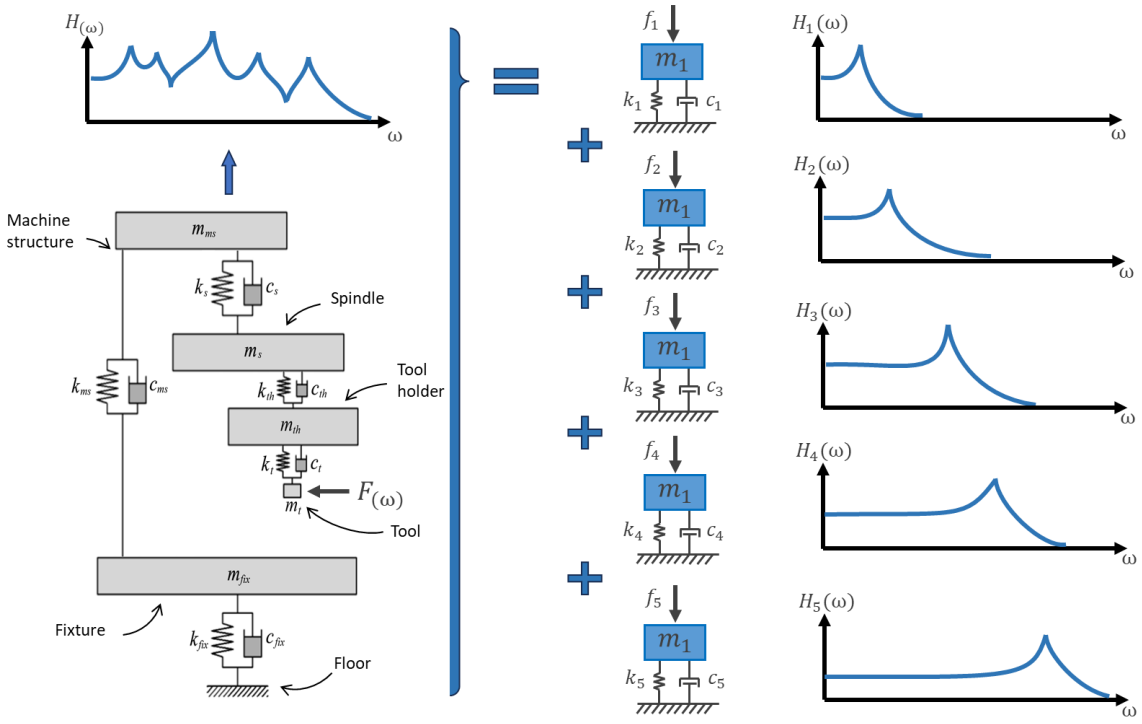

Figure 9 - Physical model to FRF model conversion.

For each natural frequency $\omega_{n(m)}$ (peaks in the imaginary part) is possible to extract each modal stiffness (k_m), mass (m_m), and damping values (ξ_m, c_m). It is important to notice that, while all modes have different parameters, system modifications will produce the same differential variation.

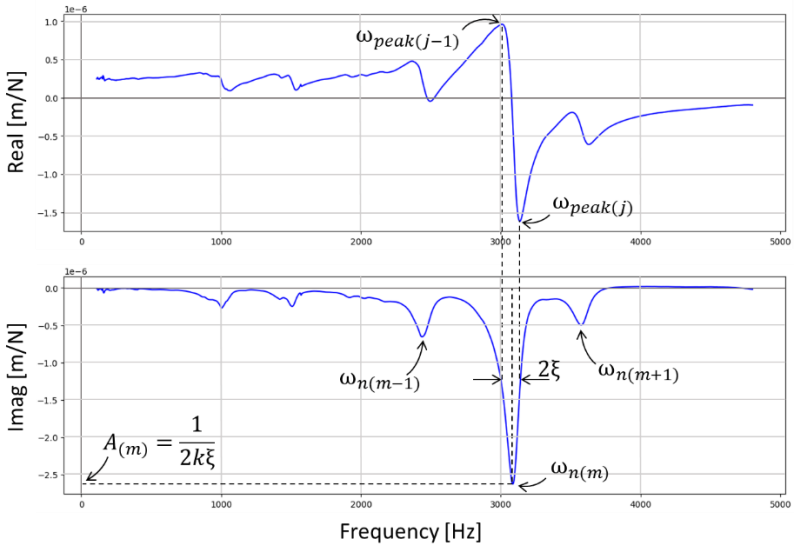

Figure 10 - Modal parameters extraction

By processing these parameters, it is possible to find the boundaries where the machine operates free of chatter vibrations, this is known as the stability lobe diagram (SLD) (Figure 11). In addition to the plot's overall description mentioned, we can distinguish an area called process-damping region. In this area, the interaction between the workpiece and the tool spinning at low velocities produce chatter mitigation. Note, as well, the peaks at high spindle speeds are “chopped”, this phenomenon is produced by the presence of flexible natural frequencies close to each other.

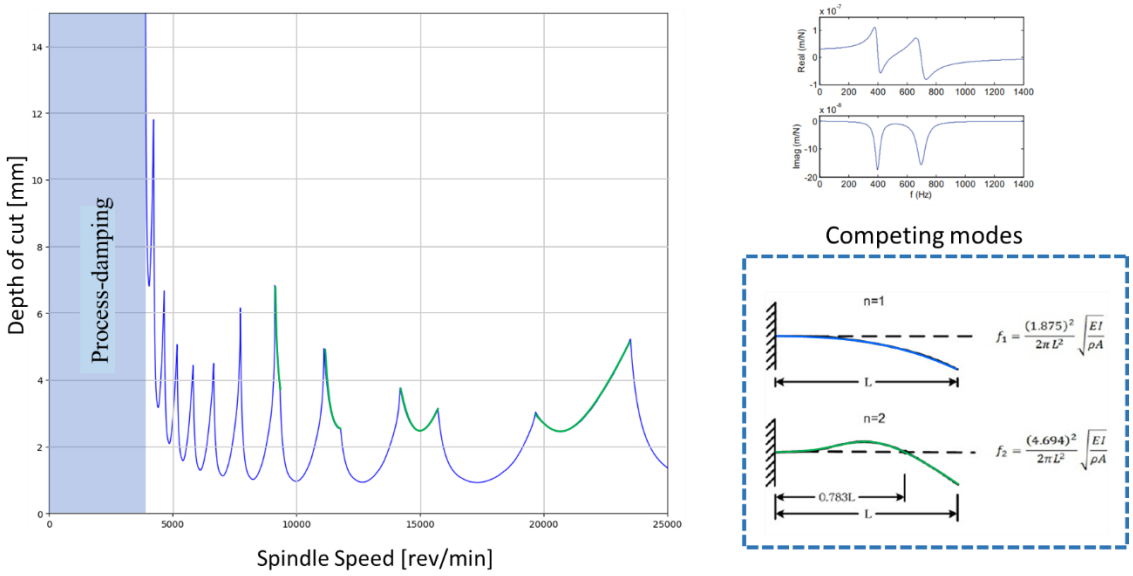

Figure 11 - General stability lobe diagram.

The result of this analysis offers the end user a solution to operate the CNC machine on the optimum stable spindle speed depth of cut combination.

Each system parameter ($\omega_{n(m)}$, k_m, m_m, ξ_m, c_m) has a specific impact on the SLD as it was studied (Li, 2017) (see Figure 12).

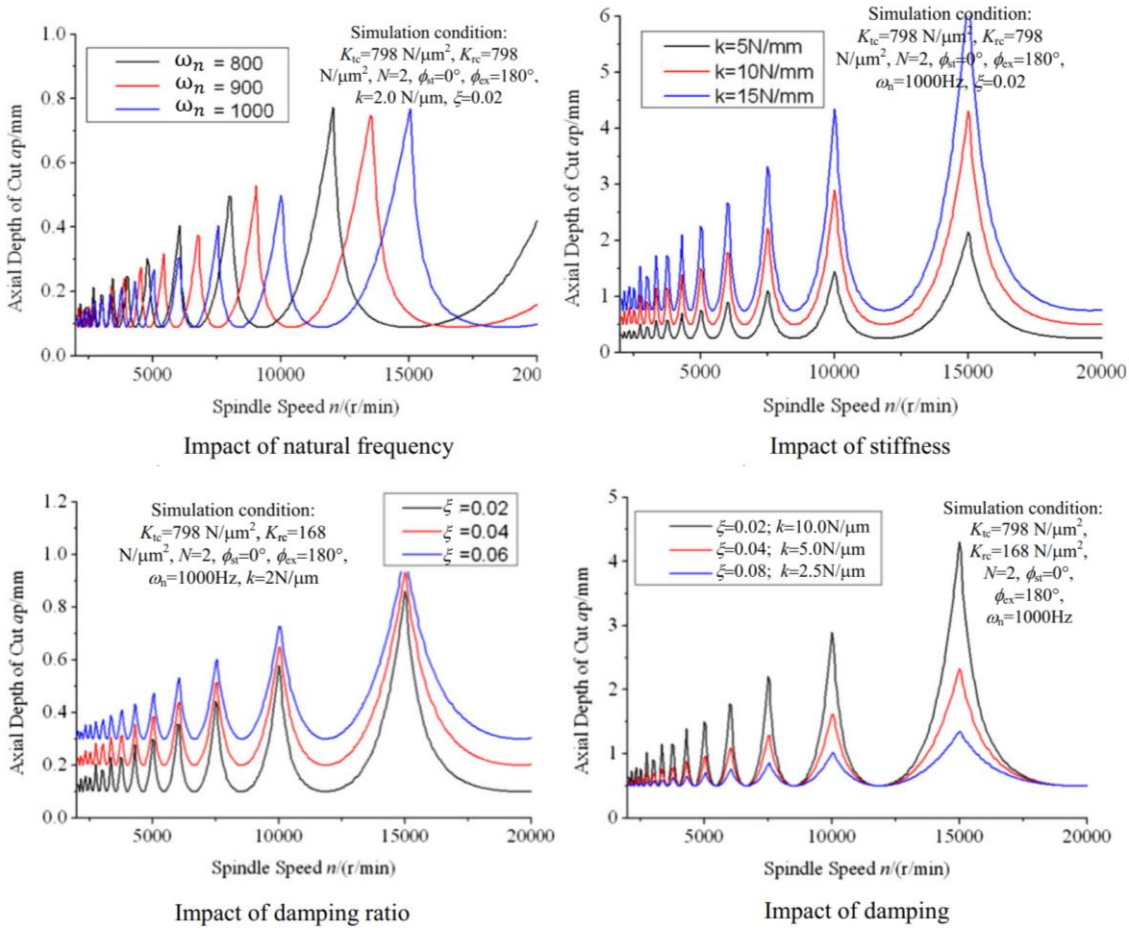

Figure 12 - Modal parameters impact on stability lobe diagram.

In these graphs, we noticed how the change in individual values of damping, natural frequency, and stiffness modifies the stability lobe diagram.

Furthermore, it was possible to observe how the specific tool configuration affects lobe shape and position (Hsiao, 2014) (see Figure 13).

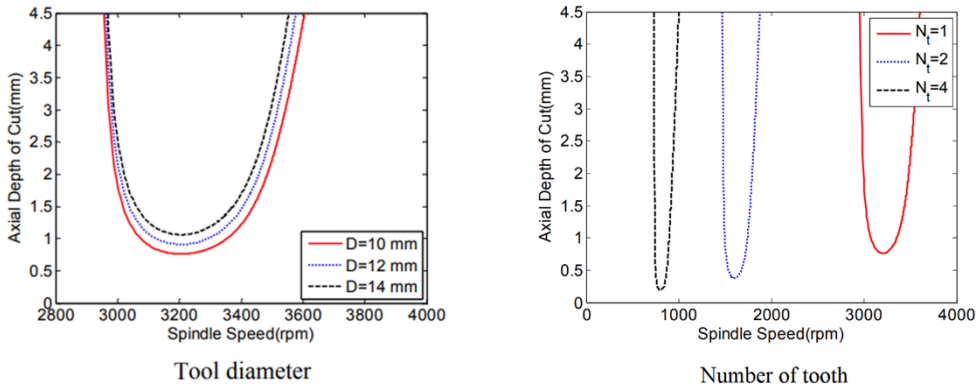

Figure 13 - Tool geometry impact on stability lobes.

The following example is more than eloquent. It is possible to see in the Table 1 (Smith, 1998) that the first choice for performing a 60 [mm] deep pocket with a Ø12,7 [mm] tool (Tools 2 and 3) would be a 70[mm] tool stickout (Extension). However, surprisingly, tests have shown selecting an 82 [mm] stickout will be two times more productive in terms of material removal rate (MRR).

Dia. (mm)	Extension (mm)	Spindle Speed (rpm)	Depth of Cut (mm)	MRR (cm^3/min)
Tool 1 - 2 Flute Ball Nose				
9.5	34	34,900	0.4	26.5
9.5	43	36,000	0.4	27.4
9.5	51	36,000	0.2	13.7
9.5	62	23,900	0.3	13.6
Tool 2 - 2 Flute 3 mm Corner Radius				
12.7	44	38,900	3.8	375.4
12.7	55	36,000	1.5	137.1
12.7	70	34,800	0.7	61.9
12.7	82	37,200	1.5	141.7
Tool 3 - 2 Flute Ball Nose				
12.7	44	38,900	2.2	217.4
12.7	55	36,000	1.3	118.9
12.7	70	34,800	0.3	26.5
12.7	82	37,200	0.7	66.1

Table 1 - Experimental data

A literature review was conducted to better understand the chatter vibration phenomena. In the Table 2, we sum up all the relevant articles read and a brief text regarding the relevance on this work.

Author (year of publication)	Relevance
Merritt (1965)	This article is one of the most important contributions to the chatter theory study. It develops the main chatter theory allowing computation of asymptotic and lobed borderlines, creating the stability lobe diagram.
Smith (1998)	This paper describes the effect of the tool length on achievable stable metal removal rate in high-speed milling. The relevant contribution to our report relies on the abundant data about natural frequency shifting and successful test cases.
Zelinski (2003)	This editorial column presents a summary of machine "sweet spot" tuning and a brief introduction to what we are currently studying. "The length by which the tool extends from the tool holder is a variable that can be used to 'tune' the machining process. Contrary to what you may expect, increasing the tool's L:D ratio may reduce chatter and result in more productive milling."
Jianping Yue (2006)	A step-by-step procedure that provides an easy way for machine operators to choose the optimum chip widths and high spindle speeds at the sweet spots on the diagram to obtain a high material removal rate. It allows us to understand the stability lobe diagram generation in the simplest possible way.
Chapra (2007)	This book was used to extract fundamental interpolation methods.
Quintana (2008)	This study is mentioned in Asier's references. While it is stated that it is used as "inspiration", one of the key points is the utilization of equipment to measure the actual chatter. This is fundamental to implementing Quintana's report. Workpiece visual inspection could work in further industry applications but there is not enough evidence to use as a research method.
Gang Jin (2013)	While this article is not related specifically to the phenomenon we are addressing in this report, it provides valuable arguments and general information for the tool selection process.
Te-Ching Hsiao (2014)	This succinct theoretical study allows us to have a better understanding of how tool parameters affect the stability lobe diagram. The evidence is valuable to verify our initial assumptions.
L. Schmitz (2016)	An important section of this report is used, through receptance substructure coupling analysis (RCSA), to study the effect of long slender tools on FRF behaviour.
Zhongqun Li (2017)	This paper is a complete study analyzing the impact of every modal parameter on the stability lobe diagram. While it's a purely theoretical analysis, the article contributes greatly to explaining the modal parameter extraction and how these

	affect the resulting SLD.
Barbeito (2020)	This analysis is one of the most complete in the field. It studies the influence of tool stickout parameters on machining stability and performs a series of practical and validation tests. The unsatisfactory conclusions (contradicting multiple practical literature) are one of the main motivations for the present report.
Bertelsen (2020)	This thesis studies the relationship between the FRF and the tool stickout and concludes with several interesting findings. This study was the baseline for the present report.
Mahboubkhah (2021)	Effect of geometrical parameters like workpiece height, thickness, tool overhang, diameter, and their ratios on the chatter stability. This paper is relevant to understand why a practical validation test performing slots on a workpiece could lead to unsatisfactory results.

Table 2 - Literature research

4 Hypothesis

Considering what we saw in “Pre-analysis and Literature search”, there are two main hypotheses for this project:

- Tailoring the tool configuration produces a change in the system FRF variables allowing the possibility of tuning the SLD at our will.
- It is possible to find a general algorithm that makes possible the optimum stickout prediction for all tools.

5 Success Criteria

To be able to find a method to predict the lobe diagram peak using data from only two tap tests would be the definition of success for this project. Nevertheless, the project's success depends on completing several mid-term goals.

- Performing the complete tap-test experiments sets.
- Accumulate enough experience in tap-test.
- Having consistent results with the selected tools.
- Finding a relationship between tool geometry and natural frequencies shifting angle.
- Having enough data volume to build a trustful model.
- Building an algorithm to recognize data series (same lobe shifting in different SLDs).

6 Project Scope/ Description

To be able to find a method to predict the lobe diagram peak using data from only two tap tests would be the definition of success for this project. Nevertheless, the project's success depends on completing several mid-term goals.

- Performing the complete tap-test experiments sets.
- Accumulate enough experience in tap-test.
- Having consistent results with the selected tools.
- Finding a relationship between tool geometry and natural frequencies shifting angle.
- Having enough data volume to build a trustful model.
- Building an algorithm to recognize data series (same lobe shifting in different SLDs).

7 Risk Analysis

Previous attempts to find a predictable relationship between stability diagrams had shown enough evidence to classify the task as challenging. During this project, DAMRC faces the following sets of risks:

- The relationship between SLDs peaks is not predictable (frequency and amplitude-wise).
- The number of tests is not enough to establish a relationship.
- Selected tools are not sensitive to stickout change.
- Stickout tooling introduces too many errors.
- Tap-Test device doesn´t produce good results.
- The experiments don’t match the SLD.
- The number of hours needed to fully develop an interpolation algorithm is not enough.

While some of the risks were mitigated by doing an extensive literature review and adjusting strategy and test setup, others depended on external factors.

- In order to avoid having problems with resolution, different test series were planned to adjust the stickout step resolution if necessary.
- To have better chances of finding interesting results tools were selected by looking at successful study cases in the literature and maximizing studied parameters.
- Tap-test device conditions were evaluated before performing every test series. Troubleshooting was contemplated in the test process. Additionally, to identify and discard unsatisfactory results the order of the experiments was recorded.
- Lastly, to address the case that the number of hours allocated to the project is not enough, all results and scope limitations were discussed in the conclusion section.

8 Design of experiments and test parts

Multiple tests were conducted on each tool varying the stickout. “Stickout tests” were the core of this project and gave us the needed data to study the effect of tool stickout on machining stability. The “Repeatability tests” were set to establish the ability to get the same response (in our case SLD) performing the same experiment. These tests gave us the standard deviations in frequency and depth of cut. All data gathered was used regardless of the goal established.

To be able to achieve the project goals it was important to establish and control all possible parameters regarding the test setup. After a survey, the following list represents the actionable factors that were controlled:

- Choice of axis: the strike was performed in just one machine axis, just rotating the spindle about the machine. [0, 90] deg.
- Stick-out deviation (tolerance of insertion).
- Hammer strike not striking the centre.
- Variance in tool clamping.
- Variance in accelerometer placement (both axial, of strike axis, and regarding asymmetrical geometry): positional methods were considered; a local axis system shall be agreed upon.
- Testing direction and position regarding the machine: a test "home point" and a strike direction were set.

All tests were performed in the most random way possible. In the realm of experimental research, particularly in this investigation, the way experiments were conducted could significantly impact the reliability and validity of the results. This methodology offered several distinct advantages that contributed to the robustness and credibility of the experimental findings.

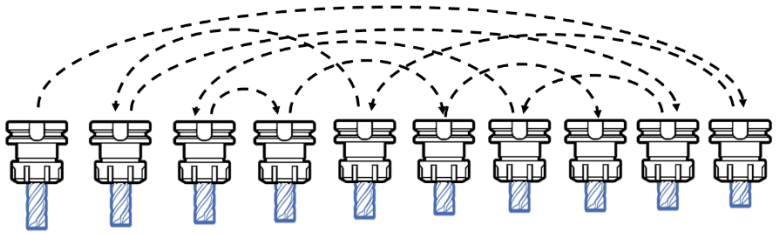

Figure 14 - Tap-test order of execution.

The random modification of stickout mitigated the introduction of bias. Predetermined sequences of setup changes can inadvertently inject bias based on prior assumptions or detailed technic. This way guaranteed that each modification was independent of previous ones, reducing the risk of such bias.

Randomization ensured comprehensive coverage of the experimental space. It enabled exploration across a wider range of possibilities, allowing the identification of potential interactions between variables that might otherwise have been overlooked.

Incorporating randomization into experimental designs was guided by a well-defined research objective and experimental plan. Proper documentation of the randomization process ensured that the results were interpretable, reproducible, and could withstand rigorous scrutiny. In summary, the use of randomly modified test setups in iterative experiments represented a valuable approach that enhanced the robustness and objectivity of research findings across various technical and scientific domains.

8.1 Repeatability tests

To have acceptable results in terms of precision and reliability it is of great importance to establish a systematic frame of work that allows us to trust in the collected data. These tests involve conducting the same experiment multiple times under identical conditions to evaluate whether the results remain consistent. The end goal of this section is to develop a systematic method to guarantee scientific validity, calibration, and data integrity.

Our main goal with this test was to take a close look at our setup. To make this happen, we were careful in how we did the test, using what we learned from past tests and what we all knew as a team. We looked at the results very closely and compared them to the rules we set beforehand. This was all to make sure that not only did the results fit within the limits we set, but they also matched the level of accuracy we aim for.

The earlier experiments conducted by DAMRC were of paramount importance as they allowed us to establish the most critical parameters. We set them up carefully to determine the best conditions for testing consistently. The accumulated experience at DAMRC enabled us to analyse mistakes and deviations, ensuring they remained within an acceptable range.

The results of this test will be important in helping us understand the system we're studying. As we move forward, we're confident that the solid foundation we've laid will support the knowledge we're working to build upon.

8.2 Stickout tap-test.

As it was written in previous sections, the analysis was focused on the “shifting” of the system behaviour frequency-wise on the SLD. As a complement, the frequency response functions (FRFs) were studied to give us a measure of the occurrence of this behaviour. However, the stability lobe diagrams will dictate how productivity can be improved by changing the stick-out, spindle speed, and depth of cut. Therefore, this experimental plan pursues to gather the necessary data to analyse which is the optimal tool stick-out to ensure not only stability while machining but also the utmost material removal rates possible (MRR).

A set of tests have been performed changing the tool stickout. To have an appropriate resolution on the analysis, and ensure at the same time, a feasible number of cases, the tool stickout varies depending on the analysed range allowed by the tool.

8.3 Tool selection

For these experiments, six different endmill tools were selected. To be able to find relationships between each other, we establish that all of them shall present similar characteristics in terms of material, shank type, and helix angle. An 8 [mm], 12 [mm], and 16 [mm] diameter tools were chosen. A duplicate set of similar tools was selected with the only difference on the flutes number. The specifications are shown in Table 3 and Table 4.

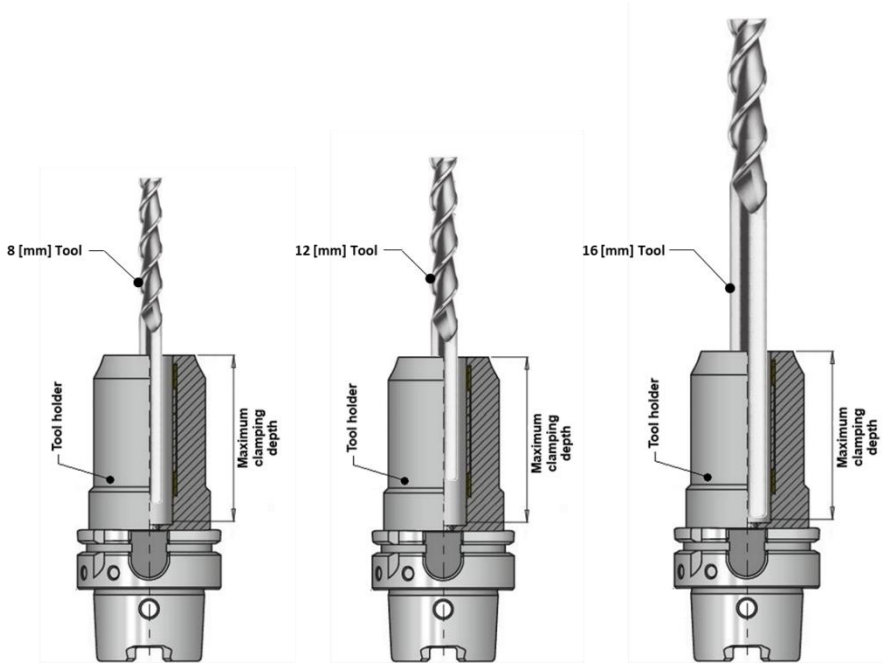

Figure 15 - Holder-tool configurations.

Part number	UA100-SL2-08040	UA100-SL2-12050	UA100-SL2-16060
Cutting diameter (DC)	8 mm	12 mm	16 mm
Depth of cut maximum (APMX)	40 mm	50 mm	60 mm
Connection diameter (DCON)	8 mm	12 mm	16 mm
Functional length (LF)	100 mm	100 mm	150 mm
Minimum Stickout	56 mm	62 mm	100 mm
Flute helix angle (FHA)	45 deg	45 deg	45 deg
Effective cutting-edge count (ZEFP)	2	2	2

Table 3 - Two flutes' tools table.

Part number	430.XL.8	430.L.12	430.L.12
Cutting diameter (DC)	8 mm	12 mm	16 mm

Depth of cut maximum (APMX)	40 mm	50 mm	60 mm
Connection diameter (DCON)	8 mm	12 mm	16 mm
Functional length (LF)	100 mm	100 mm	150 mm
Minimum Stickout	56 mm	62 mm	100 mm
Flute helix angle (FHA)	45 deg	45 deg	45 deg
Effective cutting-edge count (ZEFP)	4	4	4

Table 4 - Four flutes' tools table.

8.4 Limitations

When studying the stickout parameter it is convenient that the total tool length would be the largest possible. This gave us a bigger stickout range to investigate. Nevertheless, the following limitations were found:

- An important constraint was to find long "industry tools". This practical requirement, stated on the project application, narrows our choices down to a few available ones inside the tool catalogues.
- Another limitation is the tool cutting length, the stickout should never be reduced as much to block the chip evacuation channel.
- The available tool holders have a maximum clamping depth of 52 [mm], this imposes a limitation on the minimum stickout. One tool especially affected by this was the 16-millimeter tool, while the slenderness ratio is ideal for the study, the tool holder reduces the "potential" of this mill regarding the minimum stickout.

Two assumptions were taken to establish the maximum and minimum stickout (SO), the first one is that the maximum safe stickout will be the one that allows the tool holder to clamp the tool shaft with an insertion equivalent to at least 2 times the tool diameter. The second one was discussed earlier and is the one allowed by the tool shaft and the beginning of the tool cutting section, this limitation is set not to block the tool chip evacuation channel.

These considerations, the step resolution, together with the tool's specifications give us a certain margin on each item. Since the tools have different diameters and lengths, and these are directly related to the natural frequencies, it is convenient to use a dimensionless normalized parameter (SO:D) to handle the results.

8.5 Nomenclature

Keeping the data in a regular format is very important to streamline tests, analysis, and revision. Thus, a nomenclature for naming test experiments was created. This formatting has the additional advantages of facilitating organization, collaboration, and clarity. It's composed of the following parts:

FNNSSZZZ_TTT_VVH

Where F: tool's flutes number [2, 4].

NN: tool cutting diameter in millimetres [08, 12, 16].

SS: Y-axis measurement method, it could be filled with two values [XX or XY].

XY: if the accelerometer position was switched to measure the Y response during the tap test.

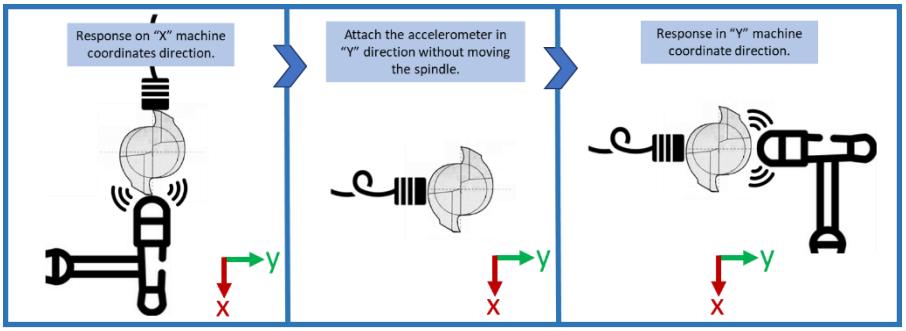

Figure 16 - Tap test XY execution.

XX: if the spindle was rotated 90 [deg] to measure the Y response during the tap test.

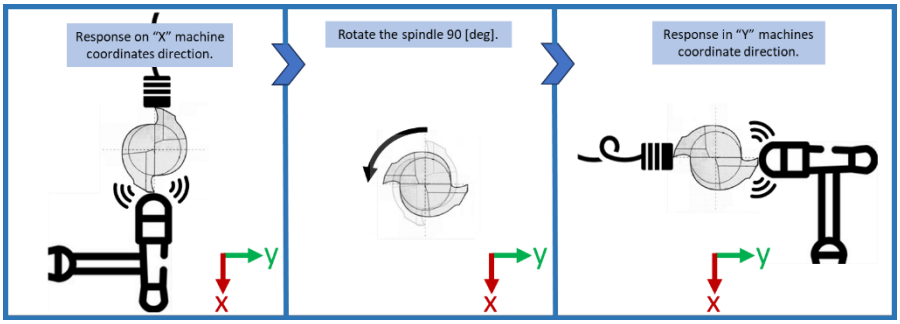

Figure 17 - Tap test XX execution.

ZZZ: tool stickout in millimetres and [056, 057, … 110]

TTT: document type [TXF, FRF, SLD]

VV: order in which the measure was taken [01, 02, … 99].

H: initial name letter of the person performing the tapping [L, S, T].

Considering that each test is composed of multiple hits (until assuring having a coherence of more than 83%) and a minimum of seven hits was agreed for each machine axis, 1600 correct hits were needed to complete all project data collection.

9 Setup of experiments

All tests used the following equipment:

- DMU 80T CNC Machine
- Torquemeter 8 [Nm]
- Tools to be tested.
- Tool holder
- Collets, 8 to 20, 12 to 20, and 16 to 20.
- 352A21 (Medium 0,6g) accelerometer.
- 8206-001 (4448 N) impact hammer, Serial Number 56482 (Brüel & Kjær) (Delrin/POM impact tip).
- Data Acquisition device.
- MetalMax TXF Software.
- Test templates for each tool analysed.
- Tool stickout MetalMax Library.

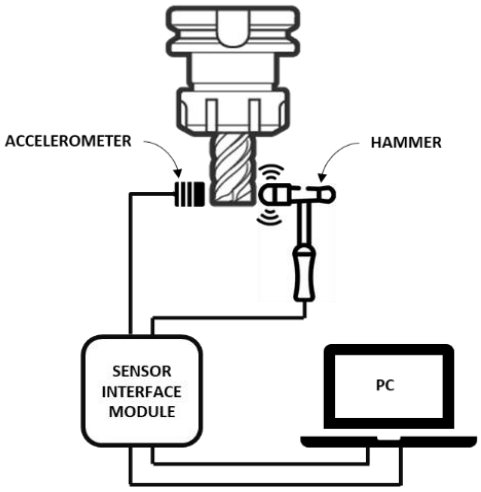

Figure 18 - Tap test components general diagram.

9.1 Library setup

To streamline the experiment setup process, a set of templates and a tool library were created. Templates are simple empty TXF files with all parameters set for each tool. The machine properties, the tool holder and the sleeve used were also part of these templates. Moreover, the software has the capacity to create all sets of tools before the experiment takes place. By reducing the need for manual parameter input, templates with preset parameters reduce the risk of human errors associated with data entry or calculation. Lastly, measurements were taken mainly by two persons, templates and preset libraries ensure that all experiments are conducted using the same standardized settings. This minimizes variations in experimental conditions, making it easier to compare and reproduce results.

10 Validate, analyses and quality assurance.

To guarantee the test results quality multiple tests on selected machine-holder-tool configurations were performed. We considered two essential parameters, coherence, and repeatability. The first one is built on in the software and is a requirement to assure the measured quality. Repeatability, on the other hand, consists of calculating the errors on frequency and depth of cut for a single machine-holder-tool configuration on different taptest sessions.

In tap tests, coherence is a measure of the consistency or correlation between input (hammer hit) and output (accelerometer measurement). Specifically, it assesses how closely related the response of a structure is to the force or excitation applied to it. Having good coherence in tap test experiments is crucial for accurate measurement, identifying natural frequencies, and mode shape determination.

The value is calculated by comparing these two data sets at different frequencies. It quantifies the relationship between the input and output signals across various frequencies. The coherence values calculated by MetalMax software can go from 0% to 100%, where a value of 100% indicates perfect correlation, meaning that the input and the output signals are perfectly related at a specific frequency. On the other hand, a value of 0% indicates no correlation, suggesting there is no relationship between input and output at a particular frequency.

In essence, coherence is a critical parameter in tap tests because it helps identify modes of vibration in a structure. It tells you how well the measured response corresponds to the excitation, which is essential for accurately characterizing a structure's dynamic behaviour and identifying potential issues such as structural damage or defects. High coherence values at specific frequencies are indicative of significant structural responses or modes.

According to best practices, for a tap test to be classified as successful, the coherence of the involved hits must be within 83%. MetalMax software allows the user for multiple (more than two) hits ensuring that the generated FRF will be sufficiently accurate.

In the Figure 19 we can appreciate a coherence followed by the flexibility plot given by MetalMax software for one of our tests. It’s important to remark that coherence value is important in the frequency range where we have the maximum flexibility amplitudes or peaks.

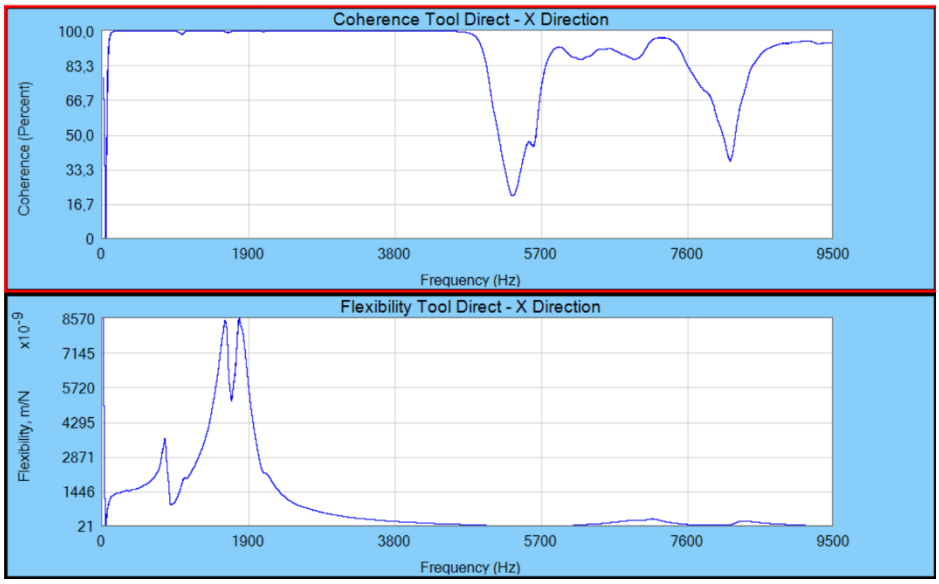

Figure 19 - Coherence and flexibility MetalMax plots.

To determine the error between measurements, several tests were plotted. Due to time limitations, the comparison was performed in just one stickout (66 [mm]) for a specific tool (408).

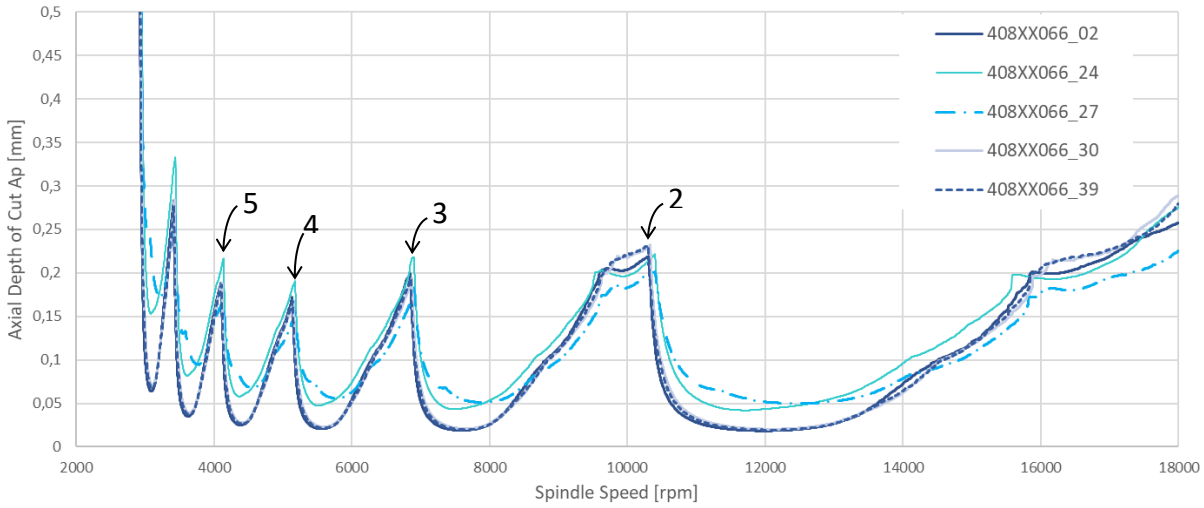

Figure 20 - Stability lobe diagram comparison.

As shown in the plot, curves presented a perfect fit and, in some cases, a considerable deviation. To establish if these deviations were going to affect our study, we had to focus our efforts on meaningful values. These values of interest are the peaks of the curve. As we developed until now, we were particularly interested in the ones closer to the maximum spindle speed. Thus, four peaks were selected, and errors were extracted.

Peak number	Test case					Avg. [Hz]	Band [Hz]	Error [%]
	02	24	27	30	39			
2	10303,2	10402,2	10405,8	10335,6	10306,8	10350,72	102,6	0,99
3	6849	6904,8	6903	6874,2	6856,2	6877,44	55,8	0,81

4	5137,2	5178,6	5184	5157	5142,6	5159,88	46,8	0,91
5	4104	4140	4143,6	4122	4109,4	4123,8	39,6	0,96

Table 5 - Frequency peaks for error calculation

As shown, frequency-wise, the error between different measures is minimum (around 1%). This is an important finding establishing limits of acceptance in our measurements. It is important noticing the deviations have certain order, meaning that the error source could be located in some systematic step (the calliper running out of zero).

Peak number	Test case					Avg. [mm]	Band [mm]	Error [%]
	02	24	27	30	39			
2	0,2188	0,2215	0,2012	0,2283	0,2293	0,21982	0,0281	12,78319
3	0,1989	0,2176	0,1834	0,1943	0,1934	0,19752	0,0342	17,3147
4	0,1784	0,1907	0,1552	0,1685	0,1672	0,172	0,0355	20,63953
5	0,1875	0,2167	0,1722	0,1884	0,1853	0,19002	0,0445	23,41859

Table 6 - Depth of cut peaks for error calculation.

In the case of depth of cut, the errors take higher values. This allowed us to mistrust or neglect this dimension. As a result of this section, it was decided to move forward on equations relating frequency shifting and leaving out of scope equations where amplitude (depth of cut) is considered.

11 Test process description.

Describing the Tap-Test test procedure in detail before conducting the experiment is essential for ensuring consistency, reproducibility, and data quality.

The following steps were followed systematically, and all details were noted:

1. Open the Metal Max TXF software.
2. Plug the cable into the USB input of the computer and the DAQ.
3. Plug the impact hammer and the accelerometer into the DAQ.
4. Attach the accelerometer to the tooltip using wax.
5. Calibrate.
6. Run a test to analyse the system conditions. Troubleshoot if necessary.
7. Do a practice, hit the tool with the hammer a couple of times until the program warns that the practice is completed.
8. Set the tool stick-out intended to analyse with the help of the digital calliper.
9. Tight the tool using the torque wrench at the test sheet torque value.
10. A new project must be set up in the Metal Max software every first test or whenever the stick-out is changed.
11. Start measuring, hit the tool in X and Y directions, and obtain their respective SLDs.

Save the original TXF file, FRF, and SLD text data. Use the format presented in the

12. Nomenclature.
13. Loop from step number 8 until completing all planned stickout.

11.1 208 Test sheet

The following test sheet (see Table 7) sums up all data collected for the 8-diameter tool. The sheet gathers three different datasets. The first one (S0) was considered a trial test, and the second dataset (S1) was conducted to refine the results by increasing the step resolution. After analysing the results and contrasting the tap test method with a specialist, it was decided to run a final setup S2, where it was decided to use method XX (see

Nomenclature).

Machine: DMU 80							
Machine setup coordinates (x, y, z) [mm]: -600, -200, 0							
Tool Holder part number: Erickson DV40HCTHT20070M							
Collet part number: 20MHC080M							
Tool part number: UA100-SL2-08040							
Clamping torque: 8 [Nm]							
Tool ID	Tool Functional Length [mm]	SO [mm]	SO/D	File names	Order		
					S0	S1	S2
208	100	56	7	208XY056_TXF_01S, 208XY056_SLD_01S, 208XY056_TXF_13S, 208XY056_SLD_13S, 208XX056_TXF_34S, 208XX056_SLD_34S	01S	13S	34S
		57	7,12	208XY057_TXF_18S, 208XY057_SLD_18S, 208XY057_TXF_39S, 208XY057_SLD_39S		18S	39S
		58	7,25	208XY058_TXF_08S, 208XY058_SLD_08S, 208XY058_TXF_24S, 208XY058_SLD_24S, 208XX058_TXF_45S, 208XX058_SLD_45S	08S		24S, 45S
		59	7,38	208XY059_TXF_20S, 208XY059_SLD_20S, 208XY059_TXF_41S, 208XY059_SLD_41S		20S	41S
		60	7,5	208XY060_TXF_04S, 208XY060_SLD_04S, 208XY060_TXF_27S, 208XY060_SLD_27S	04S		27S
		61	7,62	208XY061_TXF_16S, D08XY061_SLD_16S, 208XY061_TXF_37S, D08XY061_SLD_37S		16S	37S
		62	7,75	208XY062_TXF_06S, 208XY062_SLD_06S, 208XY062_TXF_29T, 208XY062_SLD_29T	06S		29T
		63	7,87	208XY063_TXF_21S, 208XY063_SLD_21S, 208XY063_TXF_42S, 208XY063_SLD_42S		21S	42S
		64	8	208XY064_TXF_10S, 208XY064_SLD_10S, 208XY064_TXF_31S, 208XY064_SLD_31S	10S		31S
		65	8,12	208XY065_TXF_23S, 208XY065_SLD_23S, 208XY065_TXF_44S, 208XY065_SLD_44S		23S	44S
		66	8,25	208XY066_TXF_03S, 208XY066_SLD_03S, 208XY066_TXF_14S, 208XY066_SLD_14S, D08XX066_TXF_35S, 208XX066_SLD_35S	03S	14S	35S
		67	8,37	208XY067_TXF_19S, 208XY067_SLD_19S, 208XY067_TXF_40S, 208XY067_SLD_40S		19S	40S
		68	8,5	208XY068_TXF_11S, 208XY068_SLD_11S, 208XY068_TXF_32T, 208XY068_SLD_32T	11S		32T
		69	8,62	208XY069_TXF_25S, 208XY069_SLD_25S, 208XY069_TXF_46S, 208XY069_SLD_46S			25S, 46S
		70	8,75	208XY070_TXF_07S, 208XY070_SLD_07S, 208XY070_TXF_30S, 208XY070_SLD_30S	07S		30S
		71	8,87	208XY071_TXF_15S, 208XY071_SLD_15S, 208XY071_TXF_36S, 208XY071_SLD_36S		15S	36S
		72	9	208XY072_TXF_05S, 208XY072_SLD_05S, 208XY072_TXF_28S, 208XY072_SLD_28S	05S		28S
		73	9,12	208XY073_TXF_22S, 208XY073_SLD_22S, 208XY073_TXF_43S, 208XY073_SLD_43S		22S	43S
		74	9,25	208XY074_TXF_09S, 208XY074_SLD_09S, 208XY074_TXF_26S, 208XY074_SLD_26S	09S		26S
		75	9,37	208XY075_TXF_17S, 208XY075_SLD_17S, 208XY075_TXF_38S, 208XY075_SLD_38S		17S	38S
		76	9,5	208XY076_TXF_02S, 208XY076_SLD_02S, 208XY076_TXF_12S, 208XY076_SLD_12S, 208XX076_TXF_33S, 208XX076_SLD_33S	02S	12S	33S

Table 7 - 208 Test sheet.

The data series from 40, 41, 42, 43, and 44 present disturbances in the graph, it seems all data is shifted to lower frequencies. It was found that the calliper used to take stickout measurements had the zero in a different position. Measurements were not used for analysis.

11.2 212 Test sheet

The Table 8 presents the data collected during the experiments on a 12-diameter tool. The first dataset (S0) was taken using the method XY. Due to non-satisfactory results regarding data deviation, we consider it as a trial series, and was decided to run another dataset (S1) using method XX.

Machine: DMU 80							
Machine setup coordinates (x, y, z) [mm]: -600, -200, 0							
Tool Holder part number: Erickson DV40HCTHT20070M							
Collet part number: 393.CF-201250							
Tool part number: UA100-SL2-12050							
Clamping torque: 8 [Nm]							
Tool ID	Tool Functional Length [mm]	SO [mm]	SO/D	File names	Order		
					S0	S1	S2
212	100	62	5,17	212XY062_TXF_03L, 212XY062_SLD_03L, 212XY062_TXF_06L, 212XY062_SLD_06L, 212XY062_TXF_08L, 212XY062_SLD_08L, 212XY062_TXF_18L, 212XY062_SLD_18L, 212XX062_TXF_23S, 212XX062_SLD_23S, 212XX062_TXF_25S, 212XX062_SLD_25S	03L, 06L, 08L, 18L, 23L	25S	-
		63	5,25	212XY063_TXF_14L, 212XY063_SLD_14L, 212XX063_TXF_34S, 212XX063_SLD_34S	14L	34S	-
		64	5,32	212XY064_FRF_09L, 212XY064_SLD_09L, 212XX064_FRF_36S, 212XX064_SLD_36S	09L	36S	-
		65	5,42	212XY065_TXF_22L, 212XY065_SLD_22L, 212XX065_TXF_29S, 212XX065_SLD_29S, 212XX065_TXF_30S, 212XX065_SLD_30S	22L, 29S	30S	-
		66	5,5	212XY066_TXF_04L, 212XY066_SLD_04L, 212XX066_TXF_39S, 212XX066_SLD_39S, 212XX066_TXF_40S, 212XX066_SLD_40S	04L	39S, 40S	-
		67	5,58	212XY067_TXF_12L, 212XY067_SLD_12L, 212XX067_TXF_33S, D12XX067_SLD_33S	12L	33S	-
		68	5,67	212XY068_TXF_19L, 212XY068_SLD_19L, 212XX068_TXF_27S, 212XX068_SLD_27S	19L	27S	-
		69	5,75	212XY069_TXF_02L, 212XY069_SLD_02L, 212XX069_TXF_37S, 212XX069_SLD_37S	02L	37S	-
		70	5,83	212XY070_TXF_16L, 212XY070_SLD_16L, 212XX070_TXF_35S, 212XX070_SLD_35S	16L	35S	-
		71	5,92	212XY071_TXF_20L, 212XY071_SLD_20L, 212XX071_TXF_28S, 212XX071_SLD_28S	20L	28S	-
		72	6	212XY072_TXF_07L, 212XY072_SLD_07L, 212XX072_TXF_31S, 212XX072_SLD_31S, 212XX072_TXF_32S, 212XX072_SLD_32S	07L	31S, 32S	-
		73	6,25	212XY073_TXF_11L, 212XY073_SLD_11L, 212XY073_TXF_13L, 212XY073_SLD_13L, 212XX073_TXF_38S, 212XX073_SLD_38S	11L, 13L	38S	-
		74	6,17	212XY074_TXF_01L, 212XY074_SLD_01L, 212XY074_TXF_05L, 212XY074_SLD_05L, 212XY074_TXF_10L, 212XY074_SLD_10L, 212XY074_TXF_15S, 212XY074_SLD_15S, 212XY074_TXF_17S, 212XY074_SLD_17S, 212XY074_TXF_21L, 212XY074_SLD_21L, 212XY074_TXF_24S, 212XY074_SLD_24S, 212XX074_TXF_26S, 212XX074_SLD_26S	01L, 05L, 10L, 15S, 17S, 21L	24S, 26S	-

Table 8 - 212 Test sheet.

11.3 216 Test sheet

This tool was the last to be tested. All previous experiences helped to perform just one date series (S1). The resulting data fit our expectations and we proceed directly to the analysis stage.

Machine: DMU 80							
Machine setup coordinates (x, y, z) [mm]: -600, -200, 0							
Tool Holder part number: Erickson DV40HCTHT20070M							
Collet part number: 393.CGS-201652							
Tool part number: UA100-SL2-16060							
Clamping torque: 8 [Nm]							
Tool ID	Tool Functional Length [mm]	SO [mm]	SO/D	File names	Order		
					S0	S1	S2
216	150	96	6	216XX096_TXF_02S, 216XX096_SLD_02S, 216XX096_TXF_11S, 216XX096_SLD_11S, 216XX096_TXF_20S, 216XX096_SLD_20S, 216XX096_TXF_22S, 216XX096_SLD_22S, 216XX096_TXF_26S, 216XX096_SLD_26S	-	02S 11S 20S 22S 26S	-
		97	6,06	216XX097_TXF_09S, 216XX097_SLD_09S	-	9S	-
		98	6,12	216XX098_TXF_14S, 216XX098_SLD_14S	-	14S	-
		99	6,19	216XX099_TXF_04S, 216XX099_SLD_04S	-	4S	-
		100	6,25	216XX100_TXF_07S, 216XX100_SLD_07S	-	7S	-
		101	6,31	216XX101_TXF_16S, 216XX101_SLD_16S	-	16S	-
		102	6,38	216XX102_TXF_10S, 216XX102_SLD_10S, 216XX102_TXF_13S, 216XX102_SLD_13S, 216XX102_TXF_21S, 216XX102_SLD_21S, 216XX102_TXF_24S, 216XX102_SLD_24S, 216XX102_TXF_28S, 216XX102_SLD_28S	-	10S 13S 21S 24S 28S	-
		103	6,44	216XX103_TXF_03S, 216XX103_SLD_03S	-	03S	-
		104	6,5	216XX104_TXF_18S, 216XX104_SLD_18S	-	18S	-
		105	6,56	216XX105_TXF_15S, 216XX105_SLD_15S	-	15S	-
		106	6,63	216XX106_TXF_05S, 216XX106_SLD_05S	-	5S	-
		107	6,69	216XX107_TXF_08S, 216XX107_SLD_08S	-	8S	-
		108	6,75	216XX108_TXF_17S, 216XX108_SLD_17S	-	17S	-
		109	6,81	216XX109_TXF_12S, 216XX109_SLD_12S	-	12S	-
		110	6,88	216XX110_TXF_01S, 216XX110_SLD_01S, 216XX110_TXF_06S, 216XX110_SLD_06S, 216XX110_TXF_19S, 216XX110_SLD_19S, 216XX110_TXF_23S, 216XX110_SLD_23S, 216XX110_TXF_29S, 216XX110_SLD_29S	-	01S 06S 19S 23S 29S	-
		111	6,94	216XX111_TXF_25S, 216XX111_SLD_25S	-	25S	-
		112	7	216XX112_TXF_27S, 216XX112_SLD_27S	-	27S	-

Table 9 - 216 Test sheet.

11.4 408 Test sheet

A new series of tools was tested. The experiments were taken following the accumulated experience during the two flutes tool tap tests. In the Table 10 presents the data collection for the tool using a stickout range from 56[mm] to 76[mm].

Machine: DMU 80							
Machine setup coordinates (x, y, z) [mm]: -600, -200, 0							
Tool Holder part number: Erickson DV40HCTHT20070M							
Collet part number: 20MHC080M							
Tool part number: 430.XL.8							
Clamping torque: 8 [Nm]							
Tool ID	Tool Functional Length [mm]	SO [mm]	SO/D	File names	Order		
					S1	S2	S3
408	100	56	7	408XY056_TXF_03S, 408XY056_SLD_03S, 408XY056_TXF_22S, 408XY056_SLD_22S, 408XY056_TXF_26S, 408XY056_SLD_26S, 408XY056_TXF_29S, 408XY056_SLD_29S, 408XX056_TXF_37S, 408XX056_SLD_37S	03S	22S, 26S	29S, 37S
		57	7,12	408XY057_TXF_12S, 408XY057_SLD_12S, 408XY057_TXF_43S, 408XY057_SLD_43S	12S	-	43S
		58	7,25	408XY058_TXF_09S, 408XY058_SLD_09S, 408XY058_TXF_32S, 408XY058_SLD_32S,	09S	-	32S
		59	7,38	408XY059_TXF_13S, 408XY059_SLD_13S, 408XY059_TXF_46S, 408XY059_SLD_46S	13S	-	46S
		60	7,5	408XY060_TXF_17S, 408XY060_SLD_17S, 408XY060_TXF_40S, 408XY060_SLD_40S	17S	-	40S
		61	7,62	408XY061_TXF_05S, 408XY061_SLD_05S, 408XY061_TXF_31S, 408XY061_SLD_31S	05S	-	31S
		62	7,75	408XY062_TXF_19S, 408XY062_SLD_19S, 408XY062_TXF_48S, 408XY062_SLD_48S	19S	-	48S
		63	7,87	408XY063_TXF_08S, 408XY063_SLD_08S, 408XY063_TXF_50S, 408XY063_SLD_50S	08S	-	50S
		64	8	D08XY064_TXF_10S, 408XY064_SLD_10S, D08XY064_TXF_31S, 408XY064_SLD_31S	21S	-	33S
		65	8,12	408XY065_TXF_23S, 408XY065_SLD_23S, 408XY065_TXF_44S, 408XY065_SLD_44S	15S	-	44S
		66	8,25	408XY066_TXF_02S, 408XY066_SLD_02S, 408XY066_TXF_24S, 408XY066_SLD_24S, 408XY066_TXF_27S, 408XY066_SLD_27S, 408XY066_TXF_30S, 408XY066_SLD_30S, 408XX066_TXF_39S, 408XX066_SLD_39S	02S	24S, 27S	30S, 39S
		67	8,37	408XY067_TXF_11S, 408XY067_SLD_11S, 408XY067_TXF_47S, 408XY067_SLD_47S	11S	-	47S
		68	8,5	408XY068_TXF_16S, 408XY068_SLD_16S, 408XY068_TXF_42T, 408XY068_SLD_42T	16S	-	42S
		69	8,62	408XY069_TXF_07S, 408XY069_SLD_07S, 408XY069_TXF_34S, 408XY069_SLD_34S	07S	-	34S
		70	8,75	408XY070_TXF_20S, 408XY070_SLD_20S, 408XY070_TXF_51S, 408XY070_SLD_51S	20S	-	51S
		71	8,87	408XY071_TXF_04S, 408XY071_SLD_04S, 408XY071_TXF_38S, 408XY071_SLD_38S	04S	-	38S
		72	9	408XY072_TXF_18S, 408XY072_SLD_18S, 408XY072_TXF_49S, 408XY072_SLD_49S	18S	-	49S
		73	9,12	408XY073_TXF_14S, 408XY073_SLD_14S, 408XY073_TXF_45S, 408XY073_SLD_45S	14S	-	45S
		74	9,25	408XY074_TXF_06S, 408XY074_SLD_06S, 408XY074_TXF_36S, 408XY074_SLD_36S	06S	-	36S
		75	9,37	408XY075_TXF_10S, 408XY075_SLD_10S, 408XY075_TXF_41S, 408XY075_SLD_41S	10S	-	41S
		76	9,5	408XY076_TXF_01S, 408XY076_SLD_01S, 408XY076_TXF_23S, 408XY076_SLD_23S, 408XY076_TXF_25S, 408XY076_SLD_25S, 408XY076_TXF_28S, 408XY076_SLD_28S, 408XX076_TXF_35S, 408XX076_SLD_35S	01S	23S, 25S	28S, 35S

Table 10 - 408 Test sheet.

11.5 412 Test sheet

To explore a wider range of stickouts, for this tool we have added an extended range. While this could be unpractical for actual machining it is an interesting addition to our research.

Machine: DMU 80							
Machine setup coordinates (x, y, z) [mm]: -600, -200, 0							
Tool Holder part number: Erickson DV40HCTHT20070M							
Collet part number: 20MHC120M, *393.CF-201250							
Tool part number: 430.L.12							
Clamping torque: 8 [Nm]							
Tool ID	Tool Functional Length [mm]	SO [mm]	SO/D	File names	Order		
					S1	*S2	S3
412	100	54	4,5	412XX054_TXF_09S, 412XX054_SLD_09S, 412XX054_TXF_17S, 412XX054_SLD_17S, 412XX054_TXF_26S, 412XX054_SLD_26S, 412XX054_TXF_29S, 412XX054_SLD_29S, 412XX054_TXF_32S, 412XX054_SLD_32S,	02S, 17S, 26S, 29S	32S	-
		55	4,58	412XX055_TXF_09S, 412XX055_SLD_09S,	09S	-	-
		56	4,67	412XX056_TXF_07S, 412XX056_SLD_07S,	07S	-	-
		57	4,75	412XX057_TXF_12S, 412XX057_SLD_12S,	12S	-	-
		58	4,83	412XX058_TXF_21S, 412XX058_SLD_21S,	21S	-	-
		59	4,92	412XX059_TXF_03S, 412XX059_SLD_03S,	03S	-	-
		60	5	412XX060_TXF_18S, 412XX060_SLD_18S,	18S	-	-
		61	5,08	412XX061_TXF_12S, 412XX061_SLD_12S,	11S	-	-
		62	5,17	412XX062_TXF_24S, 412XX062_SLD_24S,	24S	-	-
		63	5,25	412XX063_TXF_15S, 412XX063_SLD_15S,	15S	-	-
		64	5,32	412XX064_FRF_01S, 412XX064_SLD_01S, 412XX064_FRF_22S, 412XX064_SLD_22S, 412XX064_FRF_27S, 412XX064_SLD_27S, 412XX064_FRF_30S, 412XX064_SLD_30S, 412XX064_FRF_33S, 412XX064_SLD_33S	01S, 22S, 27S, 30S	33S	-
		65	5,42	412XX065_TXF_22S, 412XX065_SLD_22S,	06S	-	-
		66	5,5	412XX066_TXF_4S, 412XX066_SLD_4S,	08S	-	-
		67	5,58	412XX067_TXF_12S, 412XX067_SLD_12S,	16S	-	-
		68	5,67	412XX068_TXF_19S, 412XX068_SLD_19S,	23S	-	-
		69	5,75	412XX069_TXF_2S, 412XX069_SLD_2S,	05S	-	-
		70	5,83	412XY070_TXF_16S, 412XX070_SLD_16S,	13S	-	-
		71	5,92	412XX071_TXF_20S, 412XX071_SLD_20S,	20S	-	-
		72	6	412XX072_TXF_10S, 412XX072_SLD_10S	10S	-	-
		73	6,25	412XX073_TXF_14S, 412XX073_SLD_14S	14S	-	-
		74	6,17	412XY074_TXF_04S, 412XX074_SLD_04S, 412XY074_TXF_19S, 412XY074_SLD_19S, 412XX074_TXF_25S, 412XX074_SLD_25S, 412XX074_TXF_28S, 412XX074_SLD_28S, 412XX074_TXF_31S, 412XX074_SLD_31S,	04S,19S, 25S, 28S	31S	-

Table 11 - 412 Test sheet.

11.6 416 Test sheet

This tool was the last to be tested. All previous experiences helped to perform just one date series (S1). The resulting data fit our expectations and we proceed directly to the analysis stage.

Machine: DMU 80							
Machine setup coordinates (x, y, z) [mm]: -600, -200, 0							
Tool Holder part number: Erickson DV40HCTHT20070M							
Collet part number: 393.CGS-201652							
Tool part number: 430.XL.16							
Clamping torque: 8 [Nm]							
Tool ID	Tool Functional Length [mm]	SO [mm]	SO/D	File names	Order		
					S0	S1	S2
416	150	96	6	416XX096_TXF_03S, 416XX096_SLD_03S, 416XX096_TXF_15S, 416XX096_SLD_15S, 416XX096_TXF_22S, 416XX096_SLD_22S, 416XX096_TXF_25S, 416XX096_SLD_25S,	-	03S, 15S, 22S, 25S	-
		97	6,06	416XX097_TXF_18S, 416XX097_SLD_18S	-	18S	-
		98	6,12	416XX098_TXF_11S, 416XX098_SLD_11S	-	11S	-
		99	6,19	416XX099_TXF_04S, 416XX099_SLD_04S	-	04S	-
		100	6,25	416XX100_TXF_07S, 416XX100_SLD_07S	-	07S	-
		101	6,31	416XX101_TXF_20S, 416XX101_SLD_20S	-	20S	-
		102	6,38	416XX102_TXF_01S, 416XX102_SLD_01S, 416XX102_TXF_10S, 416XX102_SLD_10S, 416XX102_TXF_24S, 416XX102_SLD_24S, 416XX102_TXF_27S, 416XX102_SLD_27S,	-	01S, 10S, 24S, 27S	-
		103	6,44	416XX103_TXF_13S, 416XX103_SLD_13S	-	13S	-
		104	6,5	416XX104_TXF_09S, 416XX104_SLD_09S	-	09S	-
		105	6,56	416XX105_TXF_17S, 416XX105_SLD_17S	-	17S	-
		106	6,63	416XX106_TXF_05S, 416XX106_SLD_05S	-	05S	-
		107	6,69	416XX107_TXF_21S, 416XX107_SLD_21S	-	21S	-
		108	6,75	416XX108_TXF_14S, 416XX108_SLD_14S	-	14S	-
		109	6,81	416XX109_TXF_08S, 416XX109_SLD_08S	-	08S	-
		110	6,88	416XX110_TXF_02S, 416XX110_SLD_02S, 416XX110_TXF_19S, 416XX110_SLD_19S, 416XX110_TXF_23S, 416XX110_SLD_23S, 416XX110_TXF_26S, 416XX110_SLD_26S	-	02S, 19S, 23S, 26S	-
		111	6,94	416XX111_TXF_16S, 416XX111_SLD_16S	-	16S	-
		112	7	416XX112_TXF_06S, 416XX112_SLD_06S 416XX112_TXF_12S, 416XX112_SLD_12S	-	06S, 12S	-

Table 12 - 416 Test sheet.

12 Test results.

It is very important to be able to present the findings in a compact and clear way. While a simple superposition graph is enough to visualize the information, considering the amount of information we are gathering the presentation turns messy and confusing.

To have a better look at the frequency-shifting phenomena, two graph types were selected. A 3D surface plot allows us to pile up all data sets in one single graph and have a quick look at all results. On the other hand, to investigate in detail the behaviour, a contour-level map was chosen. These plots allow us to visualize the maximum values on the depth of cut and how this parameter changes when a modification on the stickout is introduced.

12.1 2 flutes, diameter 8 [mm] tool

This tool was the first to be tested. Thus, it was selected to do the trial tap-tests experiments. At this stage, the tap test technique has not yet been reviewed by DAMRC experts.

This gives us another angle to assess, the impact of inexperienced taptest operators on the results. The data was stored but, due to time limitations, this topic was not covered in the present report.

The Figure 21 shows the data collected using the “XX” (see

Nomenclature) method for a stickout variation from 56[mm] to 76[mm] with a step resolution of 1[mm].

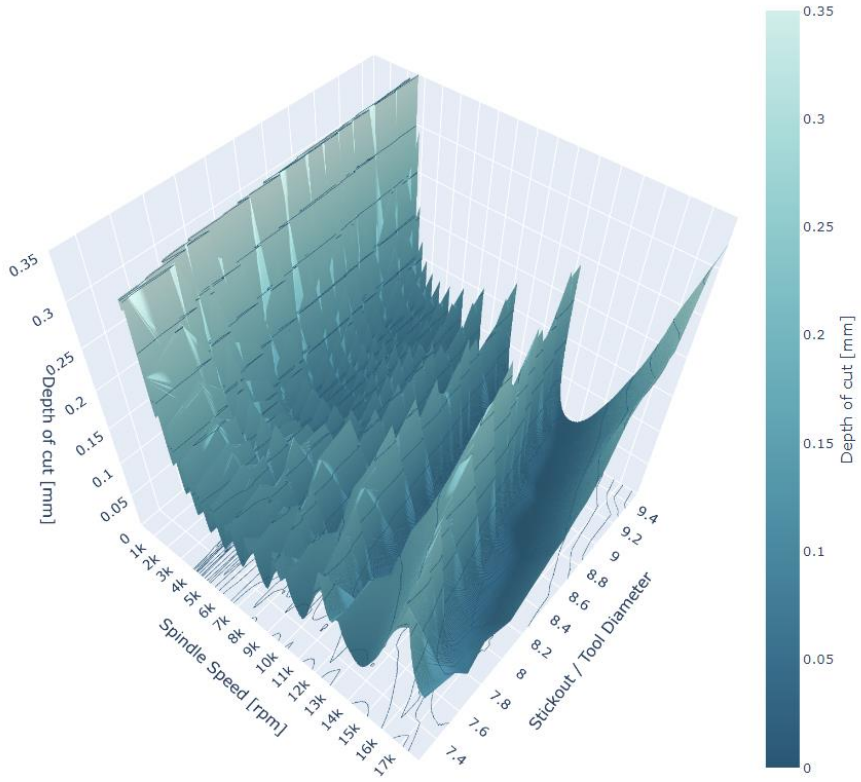

Figure 21 - 3D Stability lobe diagram on the 208 tool for different stickouts.

As we can see, the frequency shift is evident. To analyse it in depth, a contour-level map can be plotted.

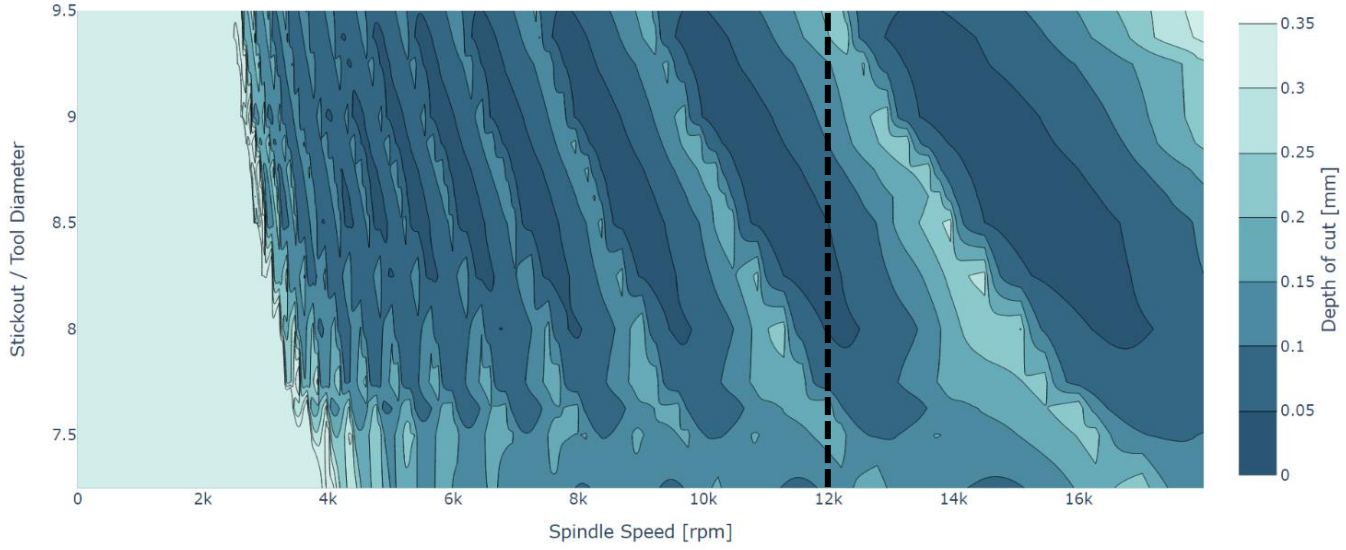

Figure 22 - Stability lobe level map for tool 208.

On the left, we can see a clear distinction between the process-damping region and the lobed region. For this report, the process-damping area is discarded due to the low material removal rates present.

12.2 2 flutes, diameter 12 [mm] tool

For this tool, the stickout variation range went from 62 [mm] to 74 [mm] with a step resolution of 1 [mm].

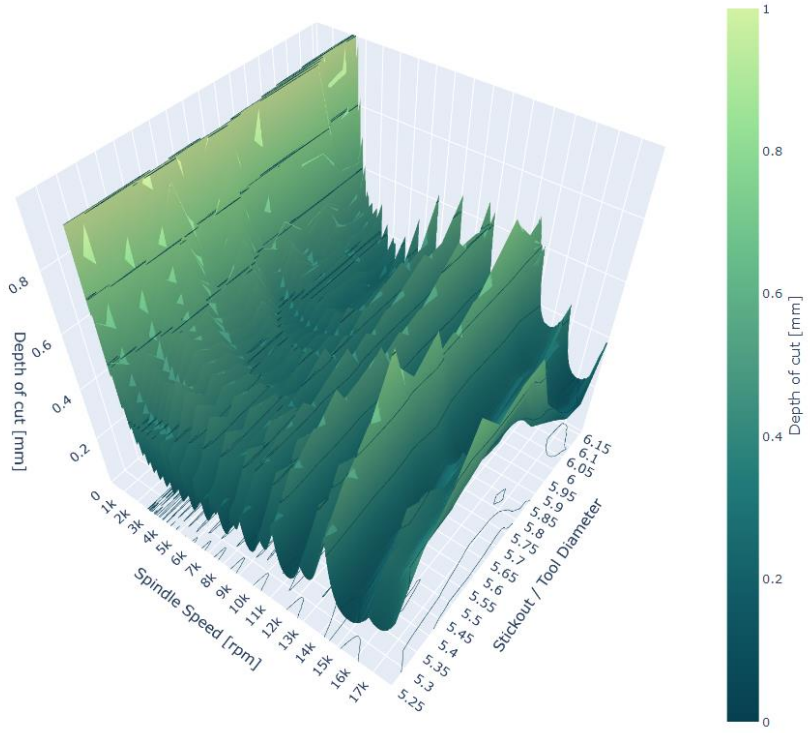

Figure 23 - 3D Stability lobe diagram on the 212 tool for different stickouts.

In this case, the frequency shifting is not evident on the 3D plot. Nevertheless, by representing the data on a contour-level graph it is possible to distinguish it.

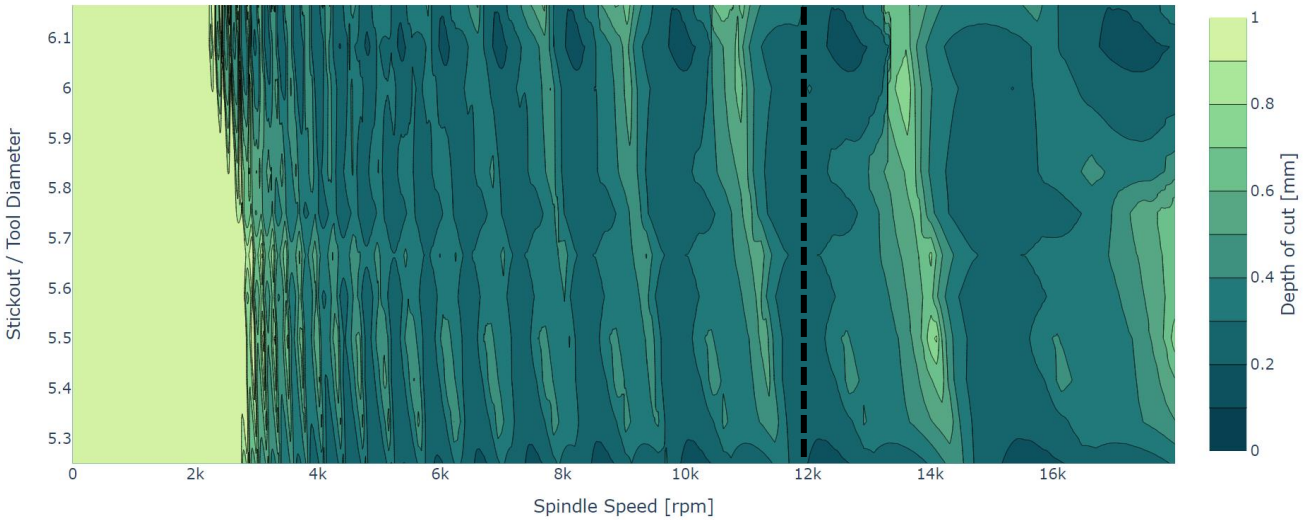

Figure 24 - Stability lobe level map for tool 212.

The variation frequency-wise is very low. In the next chapter, we will discuss the causes of this behaviour.

12.3 2 flutes, diameter 16 [mm] tool

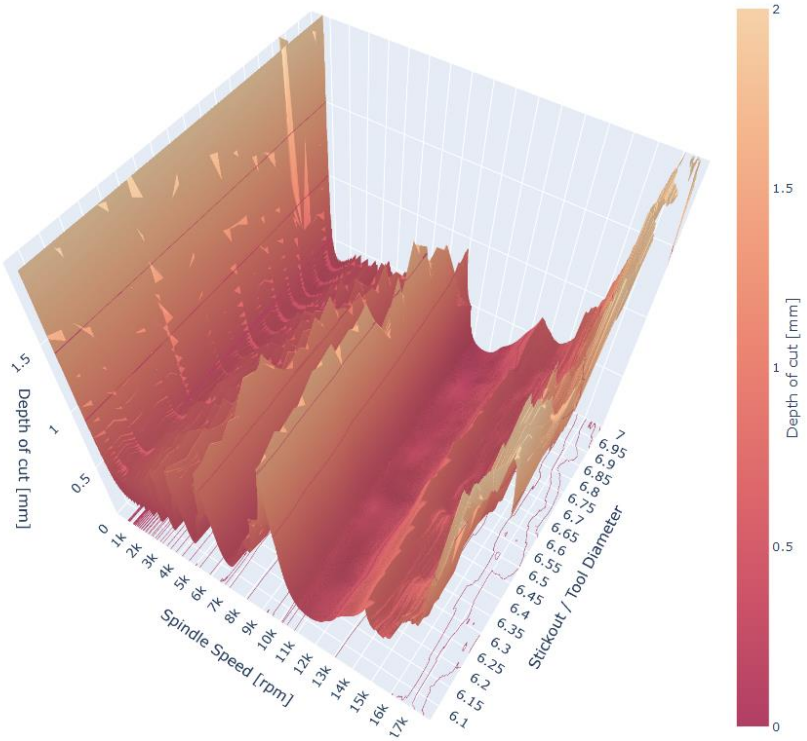

Figure 25 - 3D Stability lobe diagram on the 216 tool for different stickouts.

The case of 16 [mm] tool presents the same behaviour as the 12 [mm] tool regarding frequency shifting. No appreciable shift was observed. This limits the possible tool tunning even more, in this case, is the wide valley located at 12.000 [rpm] spindle speed (maximum machine spindle speed).

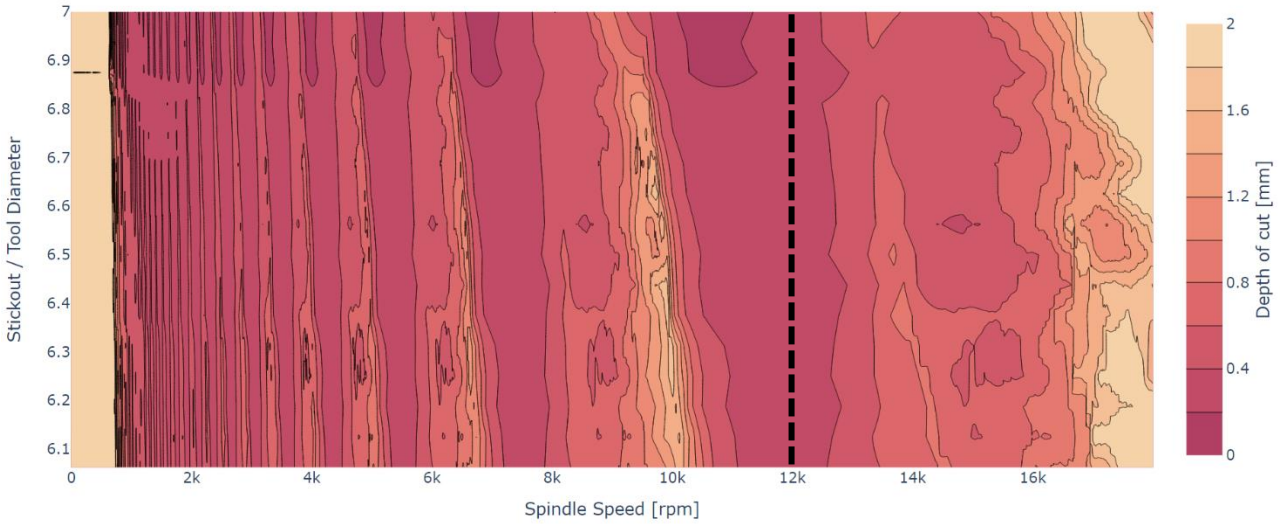

Figure 26 - Stability lobe level map for tool 212.

This characteristic makes this tool a case where it is not possible to get a better performance by changing the stickout parameter. It is important to analyse the limitations of each combination tool and tool holder system.

12.4 4 flutes, diameter 8 [mm] tool

New test sets were implemented with four flutes tools. To capture only the variation flutes variation, the tools were similar in all other aspects. The first tool analysed was an 8mm diameter. The Figure 27 shows the data collected using the “XX” (see

Nomenclature) method for a stickout variation from 56[mm] to 76[mm] with a step resolution of 1[mm].

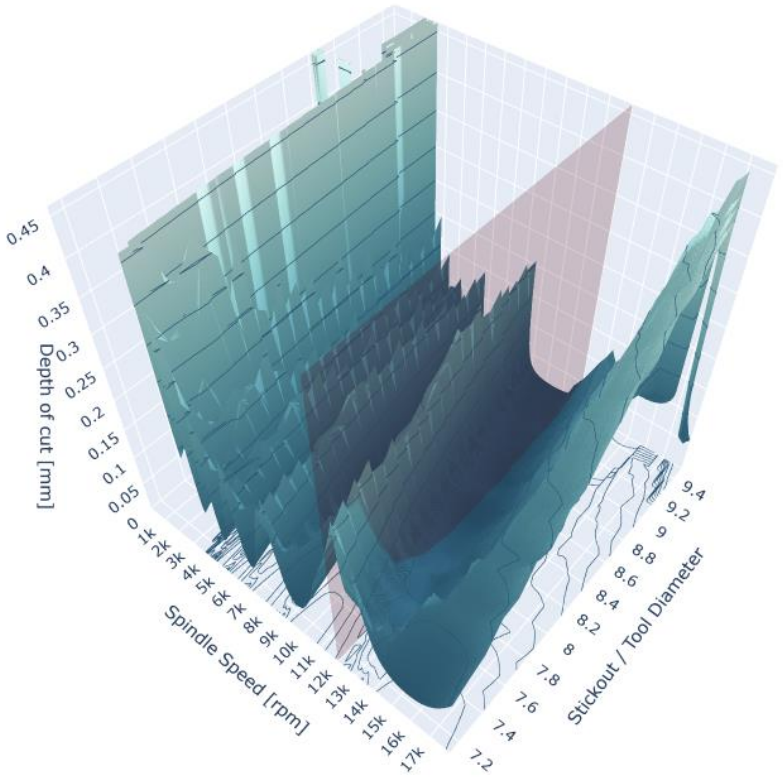

Figure 27 - 3D Stability lobe diagram on the 408 tool for different stickouts.

In this case, or this stickout range we can appreciate a lobe coincident with the maximum spindle speed at 59[mm] (SO/D=7,375). This value is very close to the minimum stickout.

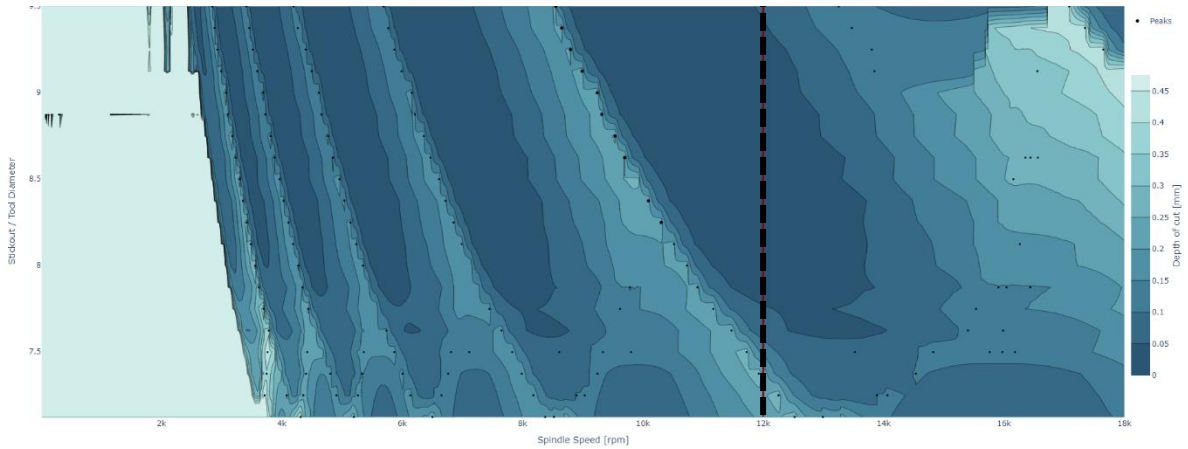

Figure 28 - Stability lobe level map for tool 408.

12.5 4 flutes, diameter 12 [mm] tool

For this tool, the stickout variation range was extended and went from 54 [mm] to 74 [mm] with a step resolution of 1 [mm]. It is worth noticing the improvement in tap test technique allowed for more consistent data resulting in an enhanced plot resolution.

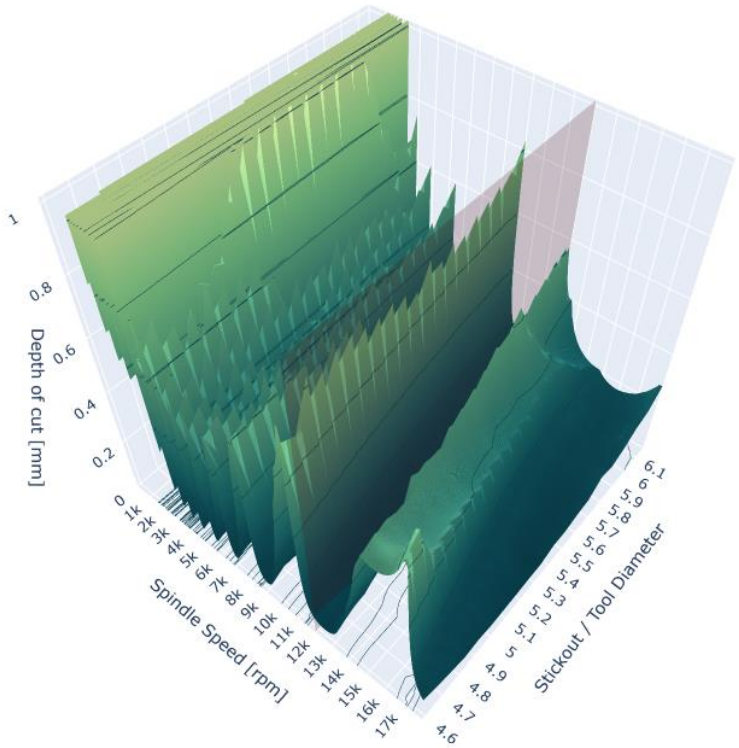

Figure 29 - 3D Stability lobe diagram on the 412 tool for different stickouts.

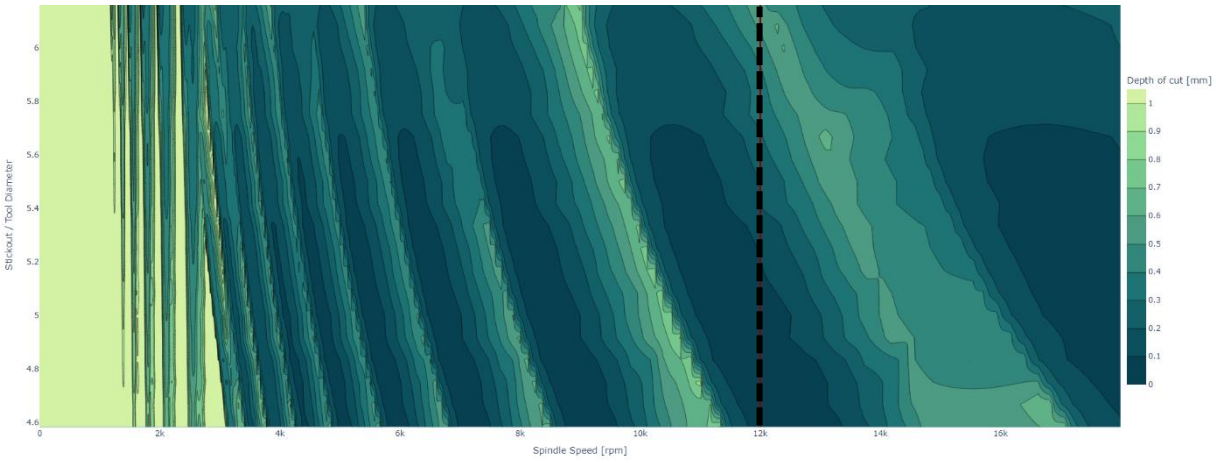

Figure 30 - Stability lobe level map for tool 412.

In this case the maximum stickout presented an area where I was possible to find a stable area close to the maximum spindle speed.

12.6 4 flutes, diameter 16 [mm] tool

The stickout variation range went from 96 [mm] to 112 [mm] with a step resolution of 1 [mm]. The tool clearly doesn't present any improvement potential. Moreover, there are no lobes after the 12000 [rpm].

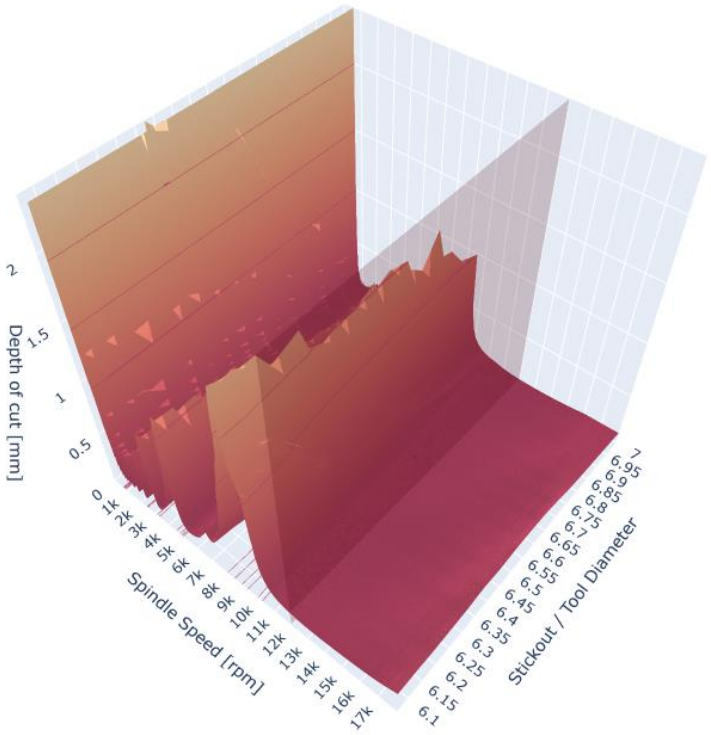

Figure 31 - 3D Stability lobe diagram on the 416 tool for different stickouts.

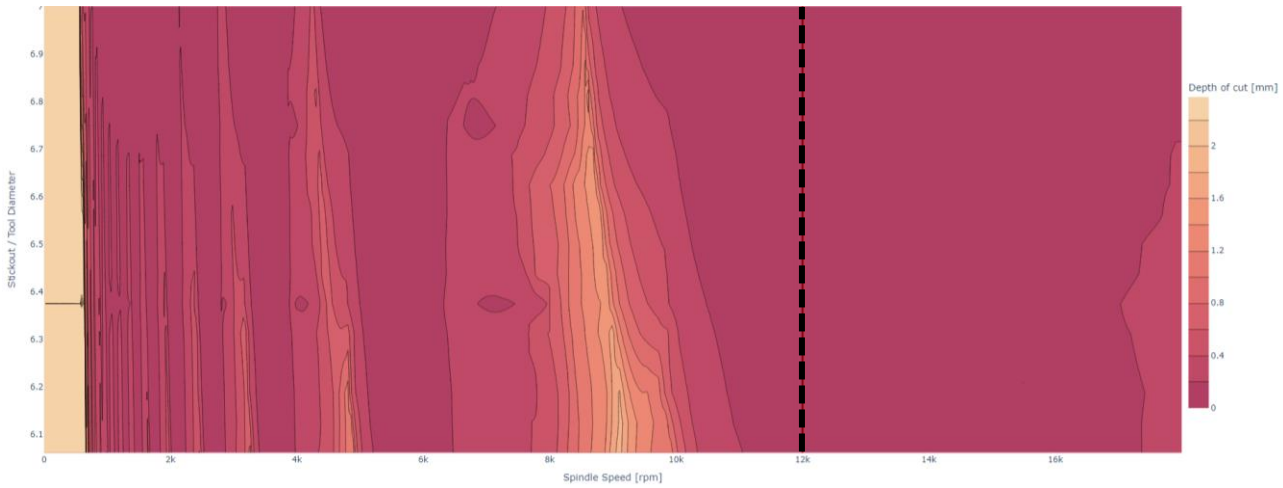

Figure 32 - Stability lobe level map for tool 416.

13 Data analysis

The analysis was divided into two sections, a general analysis of the acquired data and an analysis focused on prediction algorithm. The first of them corroborated our study hypothesis while the second aimed at the future practical application.

13.1 General analysis

In the previous chapter, results were presented allowing us to unveil the phenomenon we were anticipating. An interesting finding is that some tools have more “shifting potential” than others.

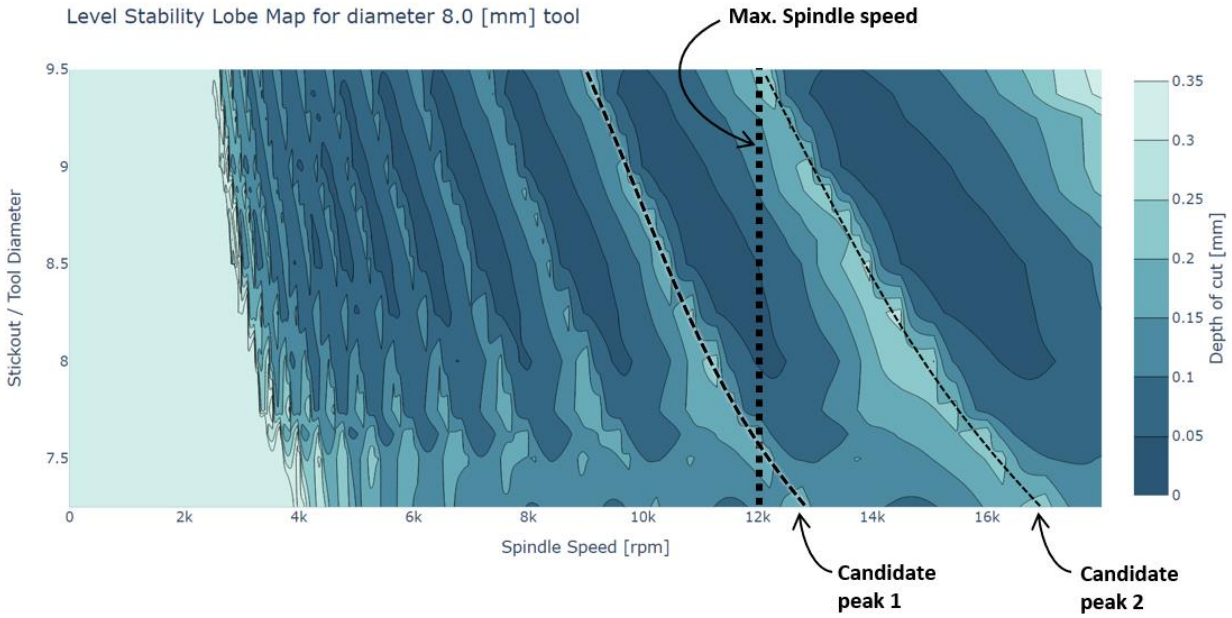

Figure 33 - Peaks shifting on tool 208.

As we can see, the 8 [mm] diameter tool possesses two different solutions (Candidate peak 1 and 2). These peaks are located approximately in stickout series 61[mm] and 76 [mm] respectively. If we take a closer look at each SLD, we can appreciate in detail the lobe characteristics.

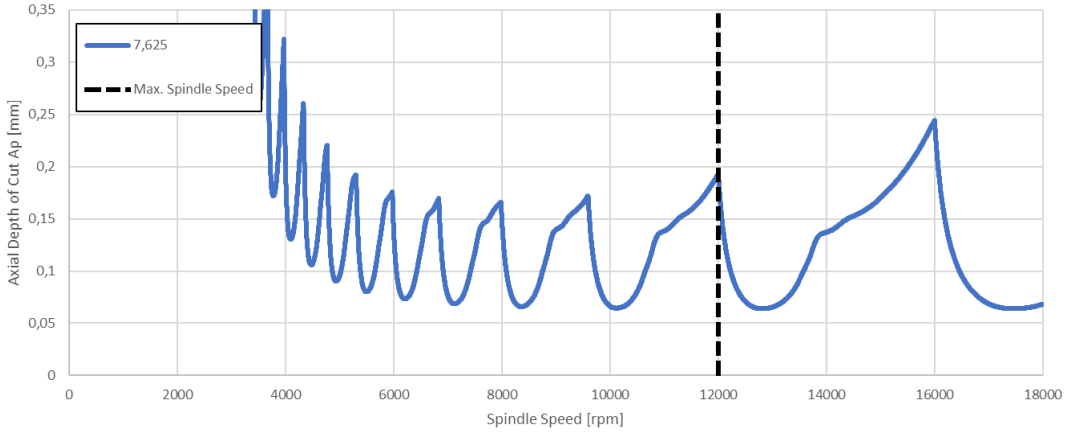

Figure 34 - Stability lobe diagram for stickout 61 [mm] (SO/D=7,625) on the 208 tool.

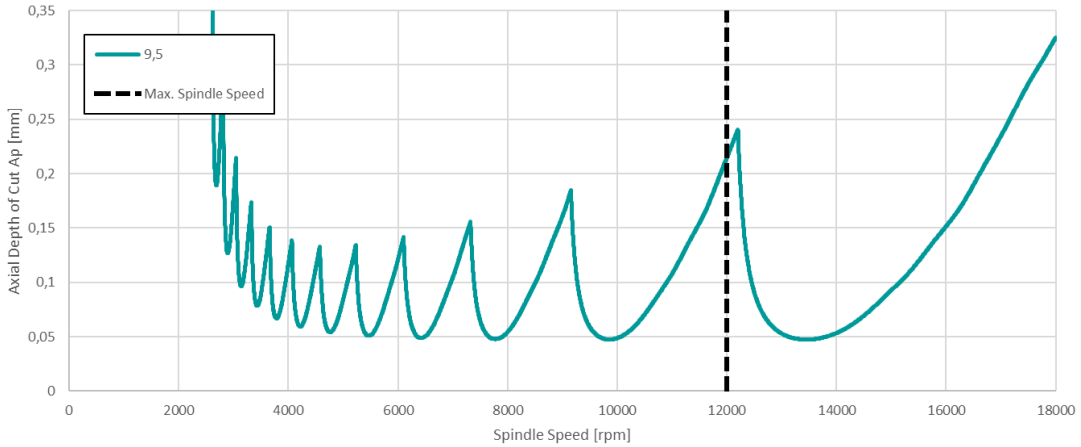

Figure 35 - Stability lobe diagram for stickout 76 [mm] (SO/D=9,5) on the 208 tool.

Both stability lobe diagrams present lobes that cross the maximum spindle speed with similar depth of cut. Even with this minimum difference in MRR, in some applications where the stickout is set (like deep pocket milling), optimizing precisely this parameter could be a game-changer.

Now, considering our previous statement “some tools have more potential than others”, it is of paramount importance to establish why this is true. In order to do it, a comparison in terms of slenderness is necessary. As we can see in the following image, the stickout ratio range Δ(SO/D) measured for the 12- and 16-millimeter tools is less than half of what we have got with the 8-millimeter tool. The main reason is tools and tool holder limitations.

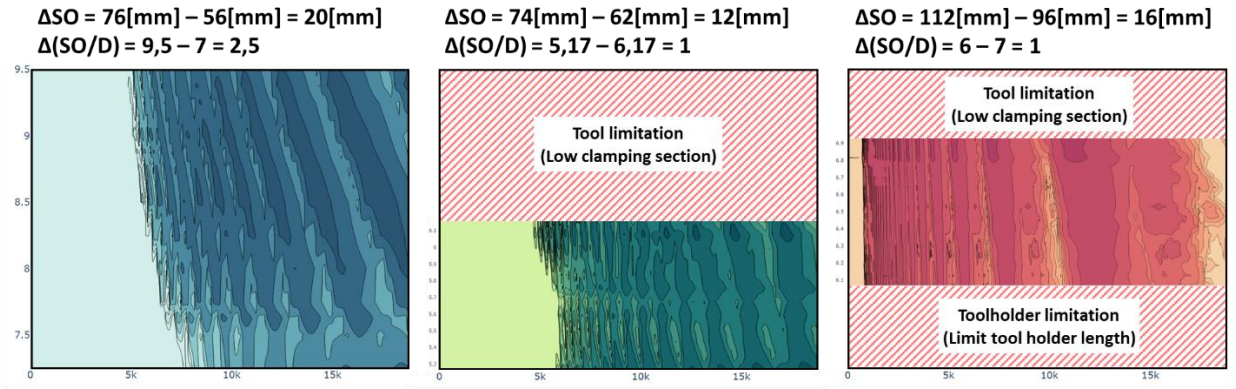

Figure 36 - General diagram on tools and holder practical limitations.

If we neglect these mechanical limitations, it is possible to see multiple stickout solutions for all tools. As an example, the peak located immediately after the maximum spindle speed on the 16-millimeter tool will intersect the maximum spindle speed at a stickout ratio of approximately 7,94 which corresponds to a stickout of 127 [mm]. The other solution for this tool, for the peak located before the maximum spindle speed, is located at 5,2 (83 [mm]).

13.2 Algorithm development

To analyse the results, due to a large amount of data, a programming code was generated. The main goal is to extract important parameters that will establish a recognizable pattern to predict the peak shifting with

the least amount of practical data. As concluded in “Validate, analyses and quality ” section, we will focus our efforts in finding frequency shifting.

This prediction would be done using interpolation or extrapolation, depending on the practical parameters introduced. In the Figure 37, the basic method is explained.

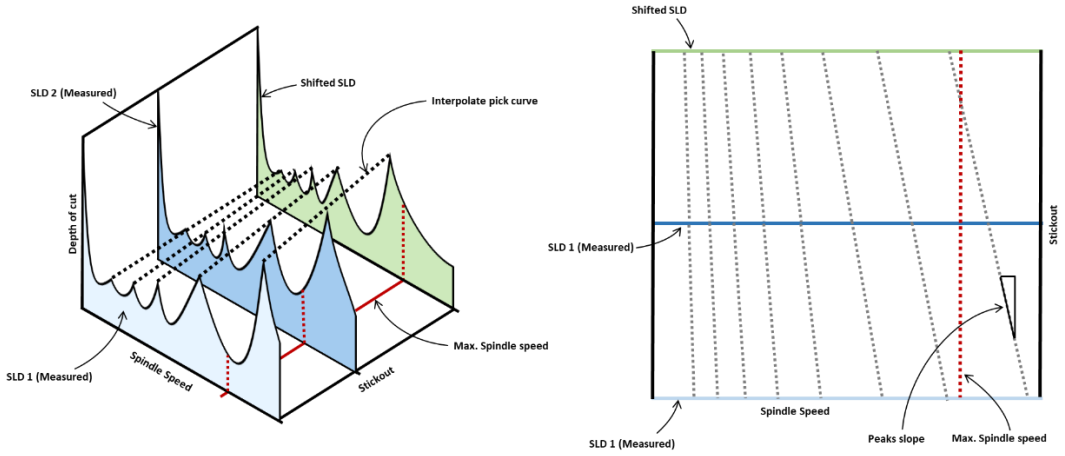

Figure 37 - Algorithm theoretical work principle.

The following flowchart describes the main algorithm's basic work principle.

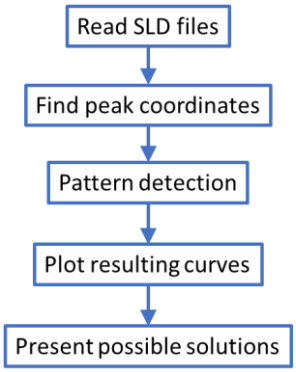

Figure 38 - Algorithm general block diagram.

Once we read all SLD files and generate the full dataset, the first step is to apply a method that allows us to find the peaks of each SLD. A slope detection code was generated; “slope sign changing” is a good way of detecting peaks and valleys. If we incorporate a restriction to capture only positive-to-negative changes, we can filtrate valleys and leave only the peaks.

This method has the advantage of not requiring any interaction on behalf of the user. The disadvantage is that the method is very sensitive to noise. To reduce the inherent sensitivity, an extra condition was introduced (e.g., only consider a peak when the last n-number of the slope average is positive and when the n-number of the following slope average is negative).

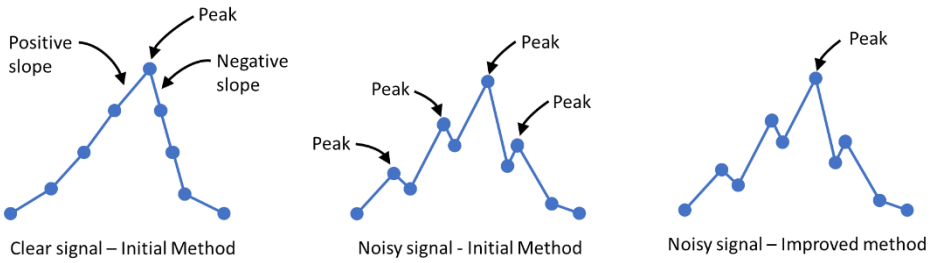

Figure 39 - Peak noise filtering.

Once the peaks are detected a way of detecting the shifting patterns is necessary. We found that shorter stickouts are prone to have competing modal frequencies that produce complicated SLDs (competing frequencies). Due to this effect, it's desirable to start iterations using mid-range stickouts.

The way of computing this pattern is to take a peak close to the maximum machine spindle speed (reference value). Once we get this first peak coordinate, we move to the next stickout dataset using the spindle speed coordinate as a reference. We calculate the closer value to this coordinate, and we continue iterating to the next stickout. After finishing with the maximum stickout, we can continue from the starting point to lower stickouts. It is important to notice we can move this reference value to capture all the other peaks sets across the different stickouts.

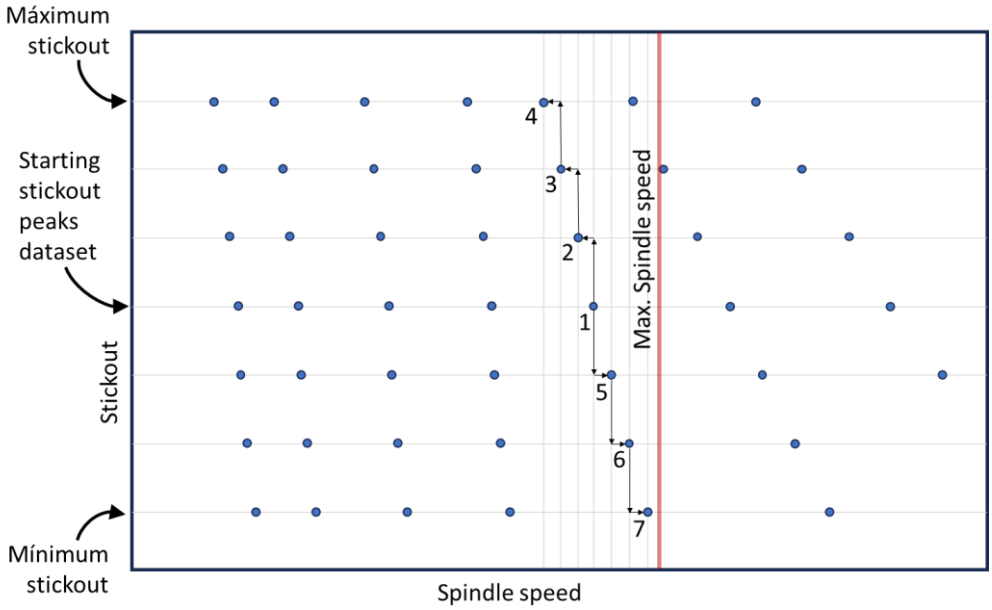

Figure 40 - Peak pattern detection.

This iteration retrieves a series of coordinates that we used to fit a curve.

13.3 Regression analysis

To choose the optimum curve, three aspects were considered, the qualitative system behaviour, how well the curve fits the values, and a physical approach. If we think about the general aspect of the phenomena, for a very long tool the natural frequencies should continue decaying and piling up with a vertical

asymptote at zero. On the other extreme, if we continue decreasing the stickout value, eventually, the frequencies will increase but the modal mass will drop to zero.

If we imagine the tool as a cantilever beam the stiffness would decrease in the inverse proportion to the cube of the length,

$$k = \frac{3EI}{l^3}$$

where E is the Young´s modulus, I is the moment of inertia, and l is the beam length. The natural frequencies would decrease in proportion to the square of the length,

$$\omega_n = 3{,}52\sqrt{\frac{EI}{\rho l^4}}$$

where ρ is the mass per unit length. We can approximate the tool as a cylinder; thus, the 2nd area moment of inertia would be,

$$I = \frac{\pi D^4}{64}$$

For systems with simple dynamics, it has been shown that stability zones occur where an integer multiple of the tooth passing frequency matches the natural frequency of the most flexible mode. That is,

$$SS = \frac{60\omega_n}{jN}$$

where j is an integer (0, 1, 2 …), and N is the number of flutes on the tool. By operating further, we get to the following expression,

$$\frac{l}{D} = \frac{5{,}138}{\sqrt{j\ D\ SS}}\sqrt[4]{\frac{E}{\rho}}$$

We can replace the l dimension with the stickout (SO) and evaluate the function for different j. In the Figure 41 we can see how the function describes the phenomenon behaviour shown in experiment results. Understanding the simplification presented in the previous equation allows us to propose different solutions.

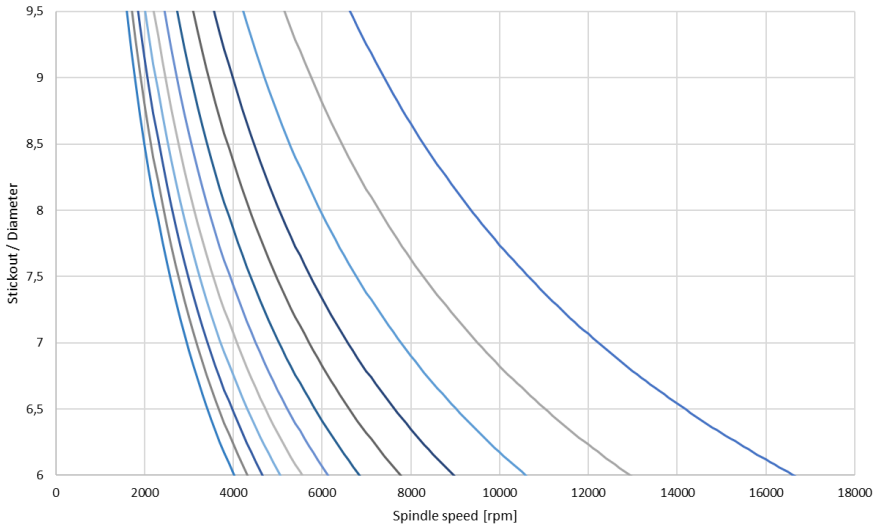

Figure 41 - Stickout Vs. Spindle Speed theoretical resulting plot.

Thus, the curve that could satisfy these three conditions would be an inverse expression like $a/\sqrt{x}+b$. The coefficients "a" and "b" is given by the fact that, in the theory, we have analyzed a simple cylinder and in practice, the system geometry has a much higher degree of complexity. To simplify the study, considering the stickout ratio range will be in most cases between 6<(SO/D)>10, it was decided to compare linear interpolation. By evaluating the fitting parameters R^2 and RMSE in the collected data, it is possible to establish the following comparison.

Tool	Inverse function	Linear
208	$SO/D = \frac{1398{,}92}{\sqrt{SS[rpm]}} - 5{,}16$	$SO/D = -\frac{6{,}245}{10000} SS[rpm] + 15{,}097$
212	$SO/D = \frac{2382{,}36}{\sqrt{SS[rpm]}} - 16{,}88$	$SO/D = -\frac{10{,}2}{10000} SS[rpm] + 17{,}061$
216	$SO/D = \frac{2221{,}8}{\sqrt{SS[rpm]}} - 15{,}44$	$SO/D = -\frac{11{,}483}{10000} SS[rpm] + 17{,}77$

Table 13 - Overview on equations shape

Tool	Inverse sqrt R^2	Inverse sqrt RMSE	Linear R^2	Linear RMSE
208	0,99	0,03	0,99	0,05
212	0,96	0,06	0,96	0,06
216	0,95	0,05	0,96	0,05

Table 14 - Error R^2 and RMSE for both regression types.

In this case, the usage of both inverse square root and linear interpolation methods yields interpolation results that are quite similar for the stickout ranges, as evidenced by the R-squared (R^2) and Root Mean Squared Error (RMSE) values for various tool sizes. The R^2 values for both interpolation methods are relatively high, indicating that both methods explain a significant proportion of the variance in the data. Additionally, the RMSE values for both methods are relatively low, suggesting that both methods provide accurate predictions when compared to the actual data.

Overall, the high R^2 values demonstrate that both interpolation methods capture the underlying trends in the data effectively. The low RMSE values indicate that both methods provide accurate predictions with

minimal error. As a result, the choice between functions, in this case, may not substantially impact the quality of the interpolated results, and both methods are valid options for interpolation depending on the specific needs and preferences of the analysis.

13.3.1 2 flutes, diameter 8 [mm] equation

To be able to calculate a single equation that describes the frequency shifting on the 8 [mm] tool we run the regression algorithm for different peaks.

Tool ID	Equation ID	Equation linear	R^2; RMSE
208	Peak j=6	$SO/D(SS) = -\frac{9{,}383}{10000}SS[rpm] + 15{,}11$	0,99; 0,07
	Peak j=5	$SO/D(SS) = -\frac{7{,}733}{10000}SS[rpm] + 15{,}05$	0,99; 0,06
	Peak j=4	$SO/D(SS) = -\frac{6{,}245}{10000}SS[rpm] + 15{,}1$	0,99; 0,07
	Peak j=3	$SO/D(SS) = -\frac{4{,}698}{10000}SS[rpm] + 15{,}12$	0,99; 0,06
	Equation inverse-square-root		
	Peak j=6	$SO/D(SS) = \frac{1144{,}73}{\sqrt{SS}} - 5{,}19$	0,99; 0,04
	Peak j=5	$SO/D(SS) = \frac{1266{,}53}{\sqrt{SS}} - 5{,}34$	0,99; 0,07
	Peak j=4	$SO/D(SS) = \frac{1398.92}{\sqrt{SS}} - 5{,}16$	0,99; 0,04
	Peak j=3	$SO/D(SS) = \frac{1616{,}82}{\sqrt{SS}} - 5{,}17$	0,99; 0,03

Table 15 - Linear and non-linear regressions for 208 tool.

The equations ID are given by the peak number j (also lobe number), and the calculation is done by solving the following equations for two different peaks in a single SLD (where there is a single ω_n),

$$SS_j = \frac{60\omega_n}{jN};\ SS_{j+1} = \frac{60\omega_n}{(j+1)N};\ \ldots;\ SS_{j+n} = \frac{60\omega_n}{(j+n)N}$$

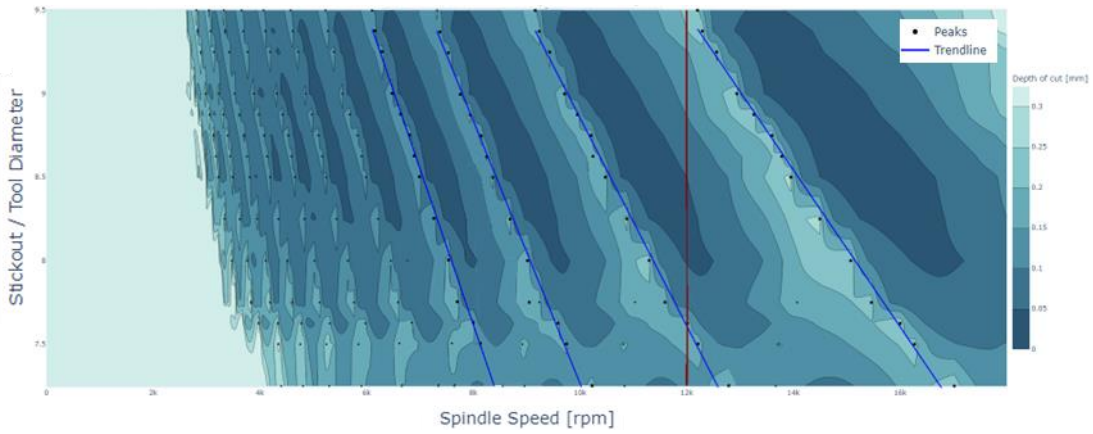

Figure 42 - Stability lobe level map with linear regression lines for tool 208.

Employing linear regression, it is possible to consider how the slope factor changes with j.

Tool ID	Equation linear	R^2
208	$SO/D\ (SS, j) = -\frac{(1{,}554j + 0{,}020)}{10000} SS[rpm] + 15{,}1$	0,99
	Equation inverse-square-root	R^2
	$SO/D\ (SS, j) = \frac{2777{,}3}{\sqrt{j\ SS}} - 5{,}21$	0,99

Table 16 - General equations for tool 208.

13.3.2 2 flutes, diameter 12 [mm] equation

Tool ID	Equation ID	Equation linear	R^2; RMSE
212	Peak j=7	$SO/D(SS) = -\frac{14{,}82}{10000} SS[rpm] + 17{,}51$	0,97; 0,04
	Peak j=6	$SO/D(SS) = -\frac{12{,}99}{10000} SS[rpm] + 17{,}77$	0,97; 0,04
	Peak j=5	$SO/D(SS) = -\frac{11{,}23}{10000} SS[rpm] + 18{,}21$	0,98; 0,04
	Peak j=4	$SO/D(SS) = -\frac{9{,}33}{10000} SS[rpm] + 18{,}69$	0,98; 0,04
	Equation inverse-square-root		
	Peak j=7	$SO/D(SS) = \frac{2130{,}82}{\sqrt{SS}} - 18{,}17$	0,97; 0,05
	Peak j=6	$SO/D(SS) = \frac{2353{,}63}{\sqrt{SS}} - 18{,}71$	0,98; 0,04
	Peak j=5	$SO/D(SS) = \frac{2669{,}88}{\sqrt{SS}} - 19{,}59$	0,98; 0,04
	Peak j=4	$SO/D(SS) = \frac{3098{,}27}{\sqrt{SS}} - 20{,}56$	0,97; 0,04

Table 17 - Linear and non-linear regressions for 212 tool.

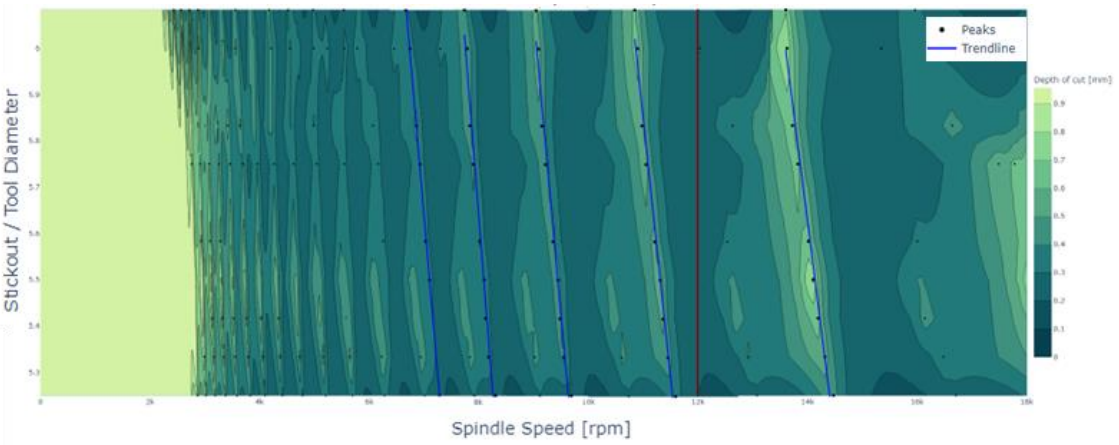

Figure 43 - Stability lobe level map with linear regression lines for tool 212.

Employing linear regression, it is possible to consider how the slope factor changes with j.

Tool ID	Equation linear	R^2
212	$SO/D\ (SS, j) = -\frac{(1{,}823j + 2{,}066)}{10000} SS[rpm] + 18{,}04$	0,99
	Equation inverse-square-root	R^2
	$SO/D\ (SS, j) = \frac{5937}{\sqrt{j\ SS}} - 19{,}25$	0,93

Table 18 - General equations for tool 212.

13.3.3 2 flutes, diameter 16 [mm] equation

Tool ID	Equation ID	Equation linear	R^2; RMSE
216	Peak j=7	$SO/D(SS) = -\frac{40{,}09}{10000} SS[rpm] + 17{,}76$	0,97; 0,05
	Peak j=6	$SO/D(SS) = -\frac{34{,}53}{10000} SS[rpm] + 17{,}83$	0,96; 0,06
	Peak j=5	$SO/D(SS) = -\frac{29{,}92}{10000} SS[rpm] + 18{,}28$	0,95; 0,06
	Peak j=4	$SO/D(SS) = -\frac{22{,}09}{10000} SS[rpm] + 17{,}41$	0,99; 0,03
	Peak j=3	$SO/D(SS) = -\frac{19{,}29}{10000} SS[rpm] + 19{,}15$	0,97; 0,04
	Peak j=2	$SO/D(SS) = -\frac{11{,}48}{10000} SS[rpm] + 17{,}77$	0,96; 0,05
	Equation inverse-square-root		
	Peak j=6	$SO/D(SS) = \frac{1076{,}92}{\sqrt{SS}} - 16{,}13$	0,99; 0,03
	Peak j=5	$SO/D(SS) = \frac{1454{,}86}{\sqrt{SS}} - 18{,}68$	0,95; 0,06
	Peak j=4	$SO/D(SS) = \frac{1509{,}38}{\sqrt{SS}} - 14{,}98$	0,99; 0,03
	Peak j=3	$SO/D(SS) = \frac{2035{,}12}{\sqrt{SS}} - 18{,}63$	0,97; 0,04

Table 19 - Linear and non-linear regressions for 216 tool.

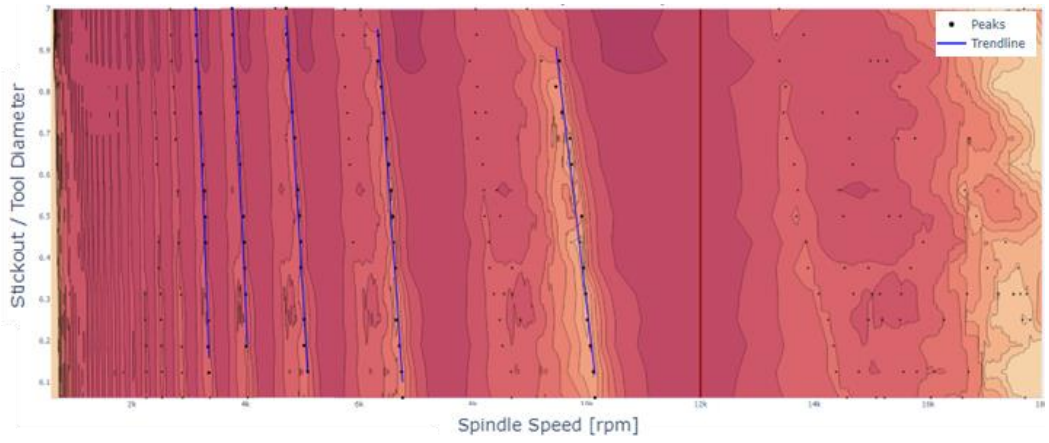

Figure 44 - Stability lobe level map with linear regression lines for tool 216.

Using linear regression, it is possible to consider how the slope factor changes with j. In this case, the intercept term presents considerable deviations when j is equal to 3 and 5. We decided to discard these equations. The resulting equation is given in the following table.

Tool ID	Equation linear	R^2
216	$SO/D\ (SS, j) = -\frac{(5{,}648j + 1{,}084)}{10000} SS[rpm] + 17{,}79$	1
	Equation inverse-square-root	R^2
	$SO/D\ (SS, j) = \frac{3178{,}9}{\sqrt{j\ SS}} - 17{,}1$	0,79

Table 20 - General equations for tool 216.

13.3.4 4 flutes, diameter 8 [mm] equation

Tool ID	Equation ID	Equation linear	R^2; RMSE
408	Peak j=6	$SO/D(SS) = -\frac{17{,}13}{10000} SS[rpm] + 14{,}2$	0,97; 0,11
	Peak j=5	$SO/D(SS) = -\frac{15{,}54}{10000} SS[rpm] + 14{,}7$	0,97; 0,07
	Peak j=4	$SO/D(SS) = -\frac{11{,}67}{10000} SS[rpm] + 14{,}33$	0,99; 0,05
	Peak j=3	$SO/D(SS) = -\frac{8{,}78}{10000} SS[rpm] + 14{,}37$	0,99; 0,07
	Peak j=2	$SO/D(SS) = -\frac{5{,}92}{10000} SS[rpm] + 14{,}43$	0,99; 0,06
	Equation inverse-square-root		
	Peak j=6	$SO/D(SS) = \frac{706{,}14}{\sqrt{SS}} - 3{,}79$	0,99; 0,05
	Peak j=5	$SO/D(SS) = \frac{765{,}63}{\sqrt{SS}} - 3{,}66$	0,99; 0,05
	Peak j=4	$SO/D(SS) = \frac{856{,}11}{\sqrt{SS}} - 3{,}67$	1; 0,03
	Peak j=3	$SO/D(SS) = \frac{1014{,}78}{\sqrt{SS}} - 3{,}98$	1; 0,02
	Peak j=2	$SO/D(SS) = \frac{1254{,}34}{\sqrt{SS}} - 4{,}10$	1; 0,02

Table 21 - Linear and non-linear regressions for 408 tool.

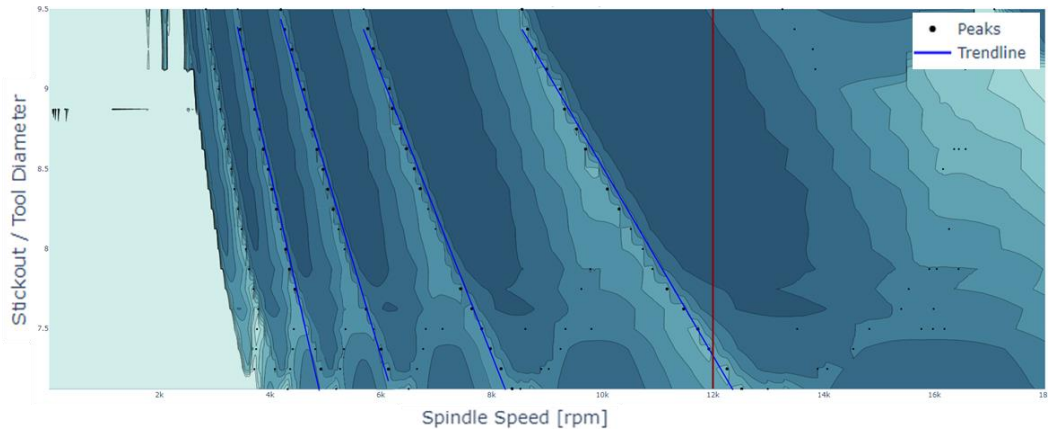

Figure 45 - Stability lobe level map with linear regression lines for tool 408.

Applying linear regression, we found the following equation that describes the different stability lobes shifting.

Tool ID	Equation	R^2
408	$SO/D\,(SS,j) = -\frac{(3{,}175j + 0{,}635)}{10000} SS[rpm] + 14{,}45$	0,99
	Equation inverse-square-root	
	$SO/D\,(SS,j) = \frac{1808}{\sqrt{j\,SS}} - 3{,}84$	

Table 22 - General equations for tool 408.

13.3.5 4 flutes, diameter 12 [mm] equation

Tool ID	Equation ID	Equation linear	R^2; RMSE
412	Peak j=7	$SO/D(SS) = -\frac{15{,}31}{10000} SS[rpm] + 11{,}92$	0,98; 0,07
	Peak j=6	$SO/D(SS) = -\frac{13{,}55}{10000} SS[rpm] + 12{,}15$	0,98; 0,07
	Peak j=5	$SO/D(SS) = -\frac{11{,}23}{10000} SS[rpm] + 12{,}10$	0,99; 0,05
	Peak j=4	$SO/D(SS) = -\frac{8{,}99}{10000} SS[rpm] + 12{,}12$	0,98; 0,07
	Peak j=3	$SO/D(SS) = -\frac{6{,}57}{10000} SS[rpm] + 11{,}94$	0,99; 0,05
	Peak j=2	$SO/D(SS) = -\frac{5{,}63}{10000} SS[rpm] + 12{,}97$	0,99; 0,04
	Equation inverse-square-root		
	Peak j=2	$SO/D(SS) = \frac{1751{,}05}{\sqrt{SS}} - 9{,}73$	0,99; 0,04
	Peak j=3	$SO/D(SS) = \frac{1330{,}58}{\sqrt{SS}} - 7{,}95$	0,99; 0,03
	Peak j=4	$SO/D(SS) = \frac{1210{,}2}{\sqrt{SS}} - 8{,}6$	0,99; 0,04

	Peak j=5	$SO/D(SS) = \frac{1050{,}83}{\sqrt{SS}} - 8{,}23$	0,99; 0,03
	Peak j=6	$SO/D(SS) = \frac{976{,}38}{\sqrt{SS}} - 8{,}45$	0,99; 0,05
	Peak j=7	$SO/D(SS) = \frac{871{,}09}{\sqrt{SS}} - 7{,}97$	0,99; 0,05

Table 23 - Linear and non-linear regressions for 412 tool.

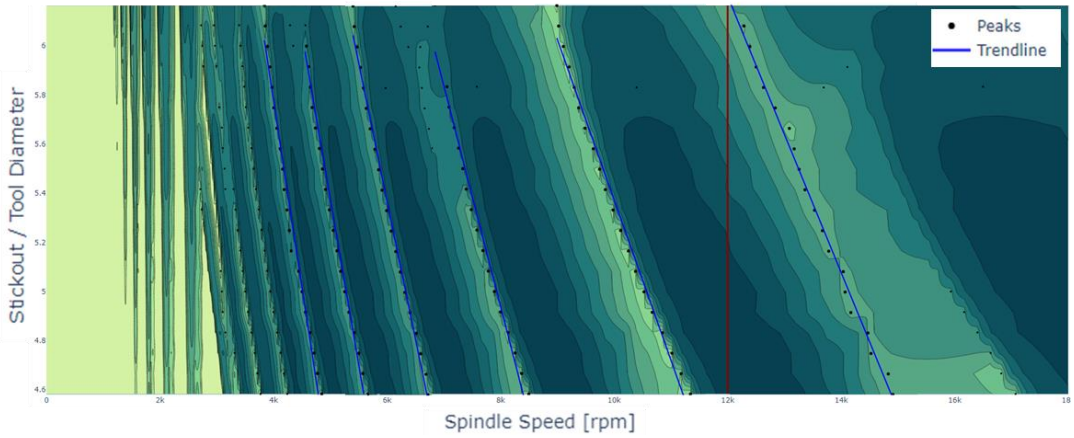

Figure 46 - Stability lobe level map with linear regression lines for tool 412.

Applying linear regression, we found the following equation that describes the different stability lobes shifting.

Tool ID	Equation	R^2
412	$SO/D\,(SS, j) = -\frac{(2{,}045j + 1{,}010)}{10000} SS[rpm] + 12{,}2$	0,99
	Equation inverse-square-root	
	$SO/D\,(SS, j) = \frac{2490{,}4}{\sqrt{j\,SS}} - 8{,}47$	0,97

Table 24 - General equations for tool 412.

13.3.6 4 flutes, diameter 16 [mm] equation

Tool ID	Equation ID	Equation linear	R^2; RMSE
416	Peak j=4	$SO/D(SS) = -\frac{26{,}31}{10000} SS[rpm] + 12{,}56$	0,98; 0,04
	Peak j=3	$SO/D(SS) = -\frac{21{,}39}{10000} SS[rpm] + 12{,}97$	0,94; 0,05
	Peak j=2	$SO/D(SS) = -\frac{14{,}59}{10000} SS[rpm] + 13{,}06$	0,91; 0,08
	Peak j=1	$SO/D(SS) = -\frac{13{,}38}{10000} SS[rpm] + 18{,}33$	0,99; 0,03
	Equation inverse-square-root		
	Peak j=4	$SO/D(SS) = \frac{579{,}63}{\sqrt{SS}} - 5{,}59$	0,98; 0,04

	Peak j=3	$SO/D(SS) = \frac{714{,}28}{\sqrt{SS}} - 6{,}49$	0,96; 0,04
	Peak j=2	$SO/D(SS) = \frac{904{,}4}{\sqrt{SS}} - 6$	0,93; 0,06
	Peak j=1	$SO/D(SS) = \frac{2220{,}35}{\sqrt{SS}} - 17{,}12$	0,99; 0,03

Table 25 - Linear and non-linear regressions for 416 tool.

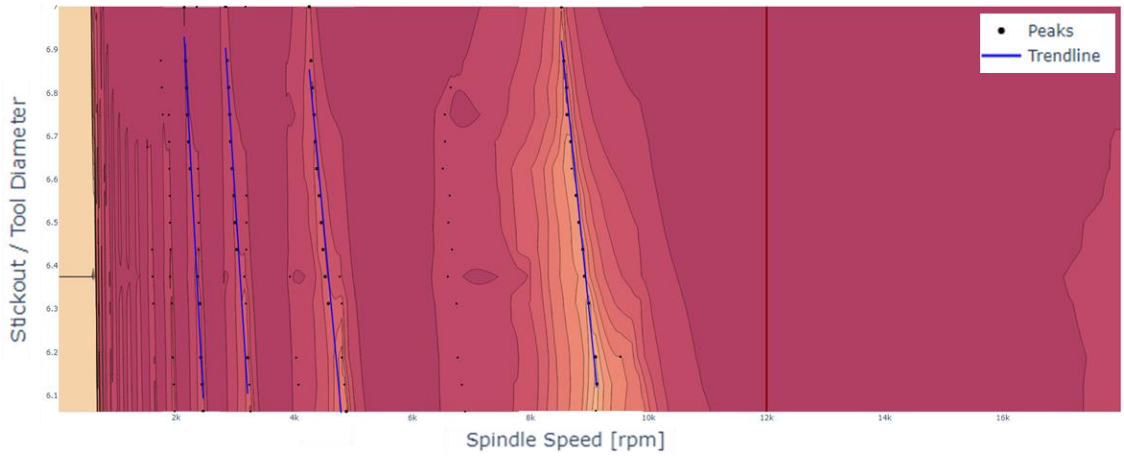

Figure 47 - Stability lobe level map with linear regression lines for tool 416.

Applying linear regression, we found the following equation that describes the different stability lobes shifting.

Tool ID	Equation linear	R^2
416	$SO/D\,(SS,j) = -\frac{(4{,}559j + 7{,}52)}{10000} SS[rpm] + 14{,}13$	0,94
	Equation inverse-square-root	0,96
	$SO/D\,(SS,j) = \frac{2059{,}1}{j\sqrt{SS}} - \frac{15{,}32}{\sqrt[5]{j^4}}$	

Table 26 - General equations for tool 416.

As we can see regressions need a higher data volume to go further. Given the number of tests performed it was not possible to continue the regression on tool diameter (D) and flutes number (Z). In both cases the amount of data is reduced to a single point for each tool. This makes the curve fitting a process where the result couldn't be trusted.

14 Conclusion

A method to predict stickout was developed on particular tool configurations. Invaluable tap test experience and insides on tool configurations were gained during the project's progress. A systematic method to collect tap test data was established giving a work frame for future research. Equations describing tool configurations were modelled and a method to get new algorithms can be extracted to advance even further.

While the end goal of this study was to create a general algorithm to predict and optimize stickout in all kinds of tools, this result ended up being too ambitious for the resources allocated to the project. A larger number of tests are required to enhance the likelihood of success. As we saw, regressions depend on data volume to enhance consistency, while data is abundant in one tool configuration, the result will always be a single equation for each tool. To relate one tool to the other and establish a general equation more tools are required.

Finally, it is important to consider the potential of this concept. During this study, we clearly saw another improvement field opening. To be able to shift lobes on the SLD opens a different approach to optimization processes, where the industry has the possibility of choosing between spindle speed or stickout variation to enhance productivity.

15 References

Hsiao, T.-C. (2014). *The Effect of Cutting Process Parameters on the Stability in Milling.*

Li, Z. (2017). *Fast prediction of chatter stability lobe diagram for milling.*

Merritt, H. E. (1965). *Theory of Self-Excited Machine-Tool Chatter.*

Oppenheim, A. V. (2012). *Señales y sistemas.*

Quintana, G. (2008). *New experimental methodology for identification of SLD in milling operations.*

Rao, S. S. (2012). *Vibraciones mecánicas.*

Schmitz, T. L. (2006.). *Tool Length-Dependent Stability Surfaces.*

Smith, S. (1998). *The Effect of Tool Length on Stable Metal Removal Rate in High Speed Milling.*

Yue, J. (2006). *Creating a Stability Lobe Diagram.*

Zelinski, P. (2003). The Overhang Effect. *Modern Machine Shop*.